INSTABILITY IN A PALLADIUM HYDRIDE SYSTEM DUE TO A FAST ELECTRICAL PERTURBATION CAUSED BY A PULSED POWER SYSTEM

A Dissertation

presented to

the Faculty of the Department of Electrical and Computer Engineering

at the University of Missouri-Columbia

In Partial Fulfillment

of the Requirements for the Degree

Doctor of Philosophy

---

by

JULIAN BAKER

Dr. John Gahl, Dissertation Supervisor

MAY 2017

The undersigned, appointed by the dean of the Graduate School, have examined the dissertation entitled

INSTABILITY IN A PALLADIUM HYDRIDE SYSTEM DUE TO A FAST ELECTRICAL PERTURBATION CAUSED BY A PULSED POWER SYSTEM

presented by Julian Baker,

a candidate for the degree of doctor of philosophy of electrical engineering,

and hereby certify that, in their opinion, it is worthy of acceptance.

Professor John Gahl

Professor Naz Islam

Professor Mahmoud Almasri

Professor Sabiha Naz

To my wife Thu.
I could not have done
this without your support.

ACKNOWLEDGEMENTS

I would like to thank everyone here at the University of Missouri who helped me during my time as a PhD student. Moreover, I would very much like to thank my advisor Professor Gahl, whose assistance and guidance were paramount to my completion of this dissertation. Additionally, I would like to show my appreciation to, Professor Islam, Professor Almasri, and Professor Naz for giving up time in their busy schedules to be part of my committee. Finally, I would like to thank Dr. Arik El-Boher, and his team here at the University of Missouri. Dr. El-Boher unselfishly gave up time in his busy schedule to answer many of my questions, and was of tremendous help in gathering resources which were vital for the completion of experiments presented in this thesis.

TABLE OF CONTENTS

LIST OF FIGURES

LIST OF TABLES

ABSTRACT

Nanoporous palladium with a specific surface area of 29.12 $m^2 g^{-1}$ was created using highly loaded palladium hydride wires subjected to a fast electrical pulse of energy. The delivered energy of approximately 0.5 J was insufficient to melt unloaded palladium wires, but in contrast, caused highly loaded palladium hydride wires to disintegrate. An element such as palladium, which was studied in these experiments, has the capacity to store hydrogen and deuterium to extremely high concentrations. Additionally, electrical explosion experiments of palladium hydride wires were performed on single samples at the loading ratios ranging from 0.5 up to 0.96, approaching the highest experimentally achieved loading ratio of 1. It was found that nanoporous palladium was created by the pulsing of palladium hydride wires at loading ratios higher than the threshold of 0.6. Each additional increase in the hydrogen loading ratio caused an accompanying increase in the surface area. In contrast, when the hydrogen loading ratio was below 0.6 the wire remained intact and there was no nanoporosity produced. Finally, a novel calorimetry technique was used to determine the relative amount of energy released from a wire during a fast, low energy pulse. Statistical analysis using Dunnett's T3 test with a significance level of 0.05 was performed on the experimental data, and showed a statistical difference between the means of the control (i.e. unloaded palladium wires) when compared to $PdH_{0.72}$ and $PdH_{0.9}$, and a statistical difference when comparing the control mean to $PdD_{0.5}$ and $PdD_{0.87}$.

Chapter 1: Introduction

Nanoporous materials have attracted considerable attention due to their critical importance in technological applications. One such material is nanoporous palladium which not only serves as a catalyst but is also useful in hydrogen storage and sensing [1-3]. For instance, the large surface to volume ratio of nanoporous palladium has been utilized in the electrocatalytic hydrogenolysis of chlorinated organic compounds [4]. A number of groups have shown that nanoporous palladium can be produced using a variety of dealloying processes [5, 6]. The evolution of the porous structure during dealloying is dominated by both the dissolution of the less noble component and surface diffusion of the more noble component. It is difficult to fully remove the less noble element in this process, leaving the residuals of less noble element in the nanoporous palladium. Additionally, nanoporous palladium powders were also synthesized by chemical reduction of tetrachloro complexes by ascorbate in a concentrated aqueous surfactant [7]. This method can produce porous structures with pore sizes of 2-3 nm.

We have discovered a novel, nonchemical, method to create nanoporous palladium through an electrical wire explosion. Others have used electrical wire explosions to produce metal nanopowders, but not nanoporous metals [8]. In our initial experiments, with the intended application to high energy density physics, deuterium loaded wires were pulsed with a low energy pulse, a so called pre-pulse, with the intent to liberate the deuterium from the wire. Surprisingly, what was discovered after the loaded wires were pulsed, was that they were converted into nanoporous palladium. On the contrary, no porosity was observed in the pulsing of palladium wires without loaded deuterium. In fact, the unloaded wires survived the pulse intact. It thus appears that the deuterium

played a critical role in the formation of nanoporous palladium. In that experiment, the highly loaded palladium deuteride wires were chemically sealed using electrodeposited mercury during electrochemical loading. After reaching high deuterium loading, a monolayer of mercury was formed on the palladium surface using electrochemical deposition. This monolayer of mercury blocks active sites for the deuterium adsorption/reduction reaction, while promoting deuterium or hydrogen absorption by inhibiting the recombination reaction [9]. Although mercury proves to be good in keeping a high deuterium loading ratio, it is toxic and can also negatively impact the effectiveness of catalysts thereby reducing the yield of reactions. Furthermore, it was not clear how the deuterium or mercury affected porosity formation in the deuterium loaded wires.

In this work, many experiments have been performed to try to gain a better understanding of the palladium hydride system. First, experiments were performed with unloaded wires, wires loaded with deuterium, and hydrogen loaded wires, and then the debris was collected so that it could be further observed using a scanning electron microscope. Next, enough highly loaded palladium hydride wires were pulsed in order to obtain surface area measurements. Lastly, to gain a better understanding of the possible physics and chemistry involved, liquid nitrogen calorimetry was used. Calorimetry has been a method explored for use in energy balance measurements for various applications in physics [10]. Following a procedure originally conducted by McKubre, et al., for pulsed dc heating of wires, the energy release from a wire after subjecting it to a fast rise time pulse was characterized [11]. The liberation of the hydrogen from the palladium at higher loading ratios should result in the release of a small amount of energy. The intent

was to utilize this diagnostic to detect this released energy. The calorimetry experiments included unloaded wires, wires loaded wire various concentrations of deuterium, wires loaded wire various concentrations of hydrogen, and wires only sealed with mercury. The details of these experiments will be explained in greater detail later in this work.

Chapter 2: The Palladium Hydride System

Palladium is a very useful metal due to its alloying ability, and is used in jewelry, dentistry, brazing alloys, and electrical contacts as well as being used as a hydrogenation catalyst [12]. Palladium has many uses which stem from its ability to store large amounts of hydrogen, which has been known since 1866 [13]. In addition to palladium readily absorbing large amounts of hydrogen, palladium can store deuterium. Hydrogen and deuterium are identical chemically, but deuterium is heavier than hydrogen being that it contains a neutron which is approximately the weight of a proton. Even so, there some interesting differences between the two. For example, after the concentration of hydrogen and deuterium increase past approximately 20%, the resistivity of the palladium deuteride is greater than the palladium hydride. *Figure 2.1* shows that deuterium has a lower zero point energy than hydrogen in the palladium lattice and therefore deuterium is more energetically favorable than hydrogen [14].

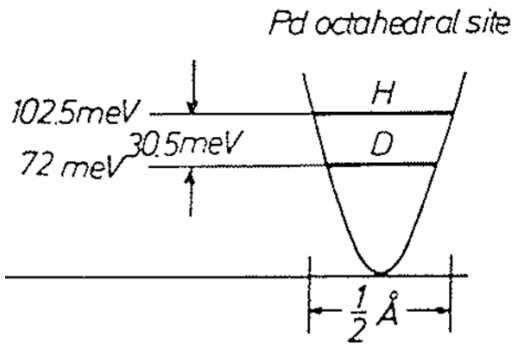

Figure 2.1: Potential well and zero-point energies of hydrogen ("H") and deuterium ("D") in the octahedral sites of palladium [14].

Another difference between hydrogen and deuterium in palladium is that their diffusion coefficients are different. *Figure 2.2* shows that the diffusion coefficient of deuterium is greater than hydrogen in palladium. This means that deuterium will move through the palladium's crystal lattice more easily than hydrogen thereby having greater mobility. Also, deuterium causes more of an increase in the lattice constant than that of hydrogen [15]. This causes an increase in strain in the deuterium loaded palladium wires. In addition to hydrogen and deuterium, palladium can store tritium, which is another isotope of hydrogen which contains two neutrons, and may be useful for future thermonuclear energy production [16].

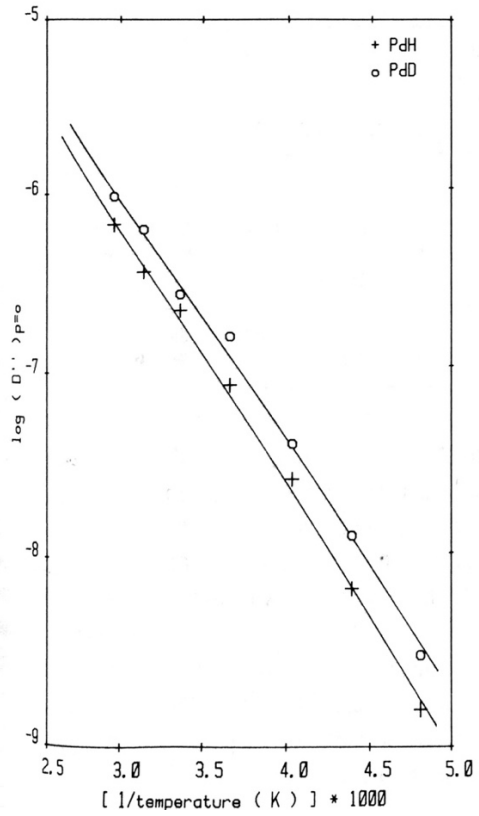

Figure 2.2: Diffusion Coefficients for hydrogen (represented by "+") and deuterium (represented by "o") [17].

Of additional interest, is how when hydrogen is absorbed into palladium, some very interesting property changes occur. For example, as the hydrogen concentration changes in the palladium, it can change from a conductor, to a semiconductor, and back to a conductor [13]. This means that the resistivity of palladium changes as a function of hydrogen loading. Hydrogen sensors are based upon this fact. For example, one palladium hydride sensor uses mesoscopic wires that, due to the change in hydrogen concentration cause a rapid decrease in the resistance of the wire array [18]. Palladium is also used in nanosensors which allow for detection of phenomenon at the nanoscale. One such nanosensor uses palladium nanoparticles placed on carbon nanotubes and the resistance changes as hydrogen is added to the sensor [19].

Another property change that occurs in palladium hydride is an increased volume that is accompanied by the increase in hydrogen concentration [13]. Additionally, the palladium undergoes what is known as hydrogen embrittlement. As the amount of hydrogen in the palladium increases, the palladium becomes less malleable and the palladium can be more easily fractured [12]. This is a major concern in hydrogen sensors where hydrogen is constantly being loaded and deloaded.

Some of the properties of palladium hydride systems are harnessed to excellent use for particular applications. For instance, even though hydrogen and its other isotopes deuterium and tritium are readily absorbed into palladium, other gases are not. This makes palladium an excellent filter allowing for separation of hydrogen gas from other gases [13]. This is done by having the gas pass through a membrane made from a palladium alloy and makes it possible to achieve purity levels greater than 99.999 % [20]. Also, through the use of catalytic ammonia decomposition, a high purity COx free

hydrogen was obtained with the use of palladium membrane walls [21]. After the hydrogen has been filtered from the other gases, it can be desorbed from the palladium to extract the hydrogen.

Another very important application of palladium is in hydrogen storage. Hydrogen has the potential of being a very important energy source in the future because it does not produce any pollutants, only water. There are however inherent difficulties with hydrogen because it must be extracted from hydrogen sources which will, of course, require energy. For hydrogen to become a viable energy source, there must be methods developed to store the hydrogen at reasonable temperatures and pressures, close to standard temperature and pressure.

2.1: Materials science of palladium hydride

Palladium that has absorbed hydrogen is referred to as palladium hydride. Interestingly, palladium hydride is not an ionic hydride, but is actually an alloy of palladium and hydrogen, which is due to its metallic bonding structure. This is also referred to as a solid solution because the structure does not change from a face centered cubic when the hydrogen is added. Palladium metal has a crystal structure that is face centered cubic (FCC). When hydrogen is absorbed into the palladium, it occupies interstitial octahedral sites in the palladium lattice as shown in *Figure 2.3*.

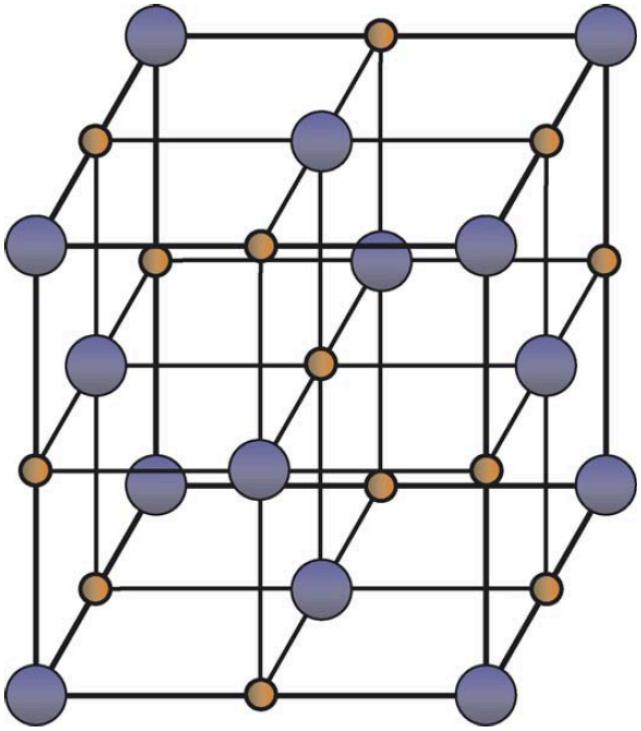

Figure 2.3: Face centered cubic structure of palladium hydride [22].

Palladium hydride has two distinct phases: alpha and beta phase. *Figure 2.4* shows both the alpha and beta phases as a function of temperature and hydrogen concentration. When palladium hydride is in the alpha phase, the structure of the palladium metal stays the same; however, the lattice constant increases slightly with increasing hydrogen concentration. As loading is increased while in the alpha phase, the crystal lattice structure becomes unstable until there is a large jump in the lattice constant. After this jump in the lattice constant occurs, the palladium hydride is in the beta phase. When the palladium hydride is in the beta phase, again the structure of the palladium metal stays the same, but the lattice constant increases by a much larger amount than in the alpha phase (up to 10%).

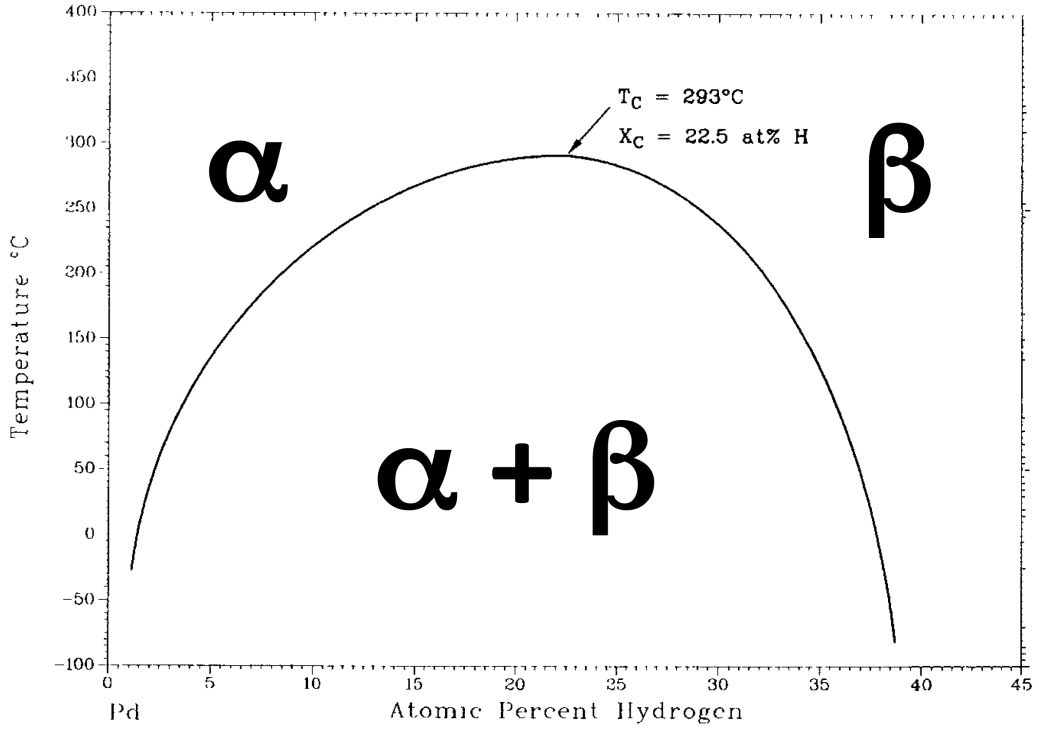

Figure 2.4: Alpha and Beta phases of palladium hydride [23].

Figure 2.5 (a) shows the interstitial locations that hydrogen atoms occupy in the palladium lattice while in the alpha phase, and *Figure 2.5* (b) shows the interstitial locations the hydrogen atoms occupy in the palladium lattice while in the beta phase. Notice that while in the alpha phase the hydrogen atoms appear to occupy the octahedral sites in the lattice randomly, while in the beta phase the hydrogen atoms cluster together.

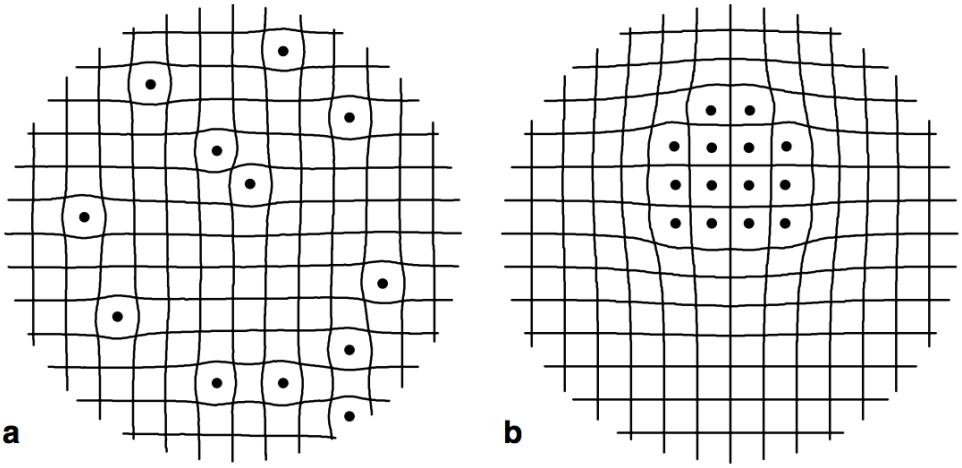

Figure 2.5: (a) shows the locations of hydrogen atoms in the palladium lattice during the alpha phase. (b) shows the locations of hydrogen atoms in the palladium lattice in the beta phase [24].

Figure 2.6 is a pressure concentration isotherm, where each line is a constant temperature, the vertical axis is pressure, and the horizontal axis is the atomic ratio H/Pd. This figure shows that to achieve very highly loaded palladium using gas loading would require a very low temperature, otherwise the pressure required would be enormous. For example, at 477 °C to achieve 60 percent loading would require 1000 atm of pressure, whereas at -78 °C an 87 percent loading can occur at 1 atm of pressure.

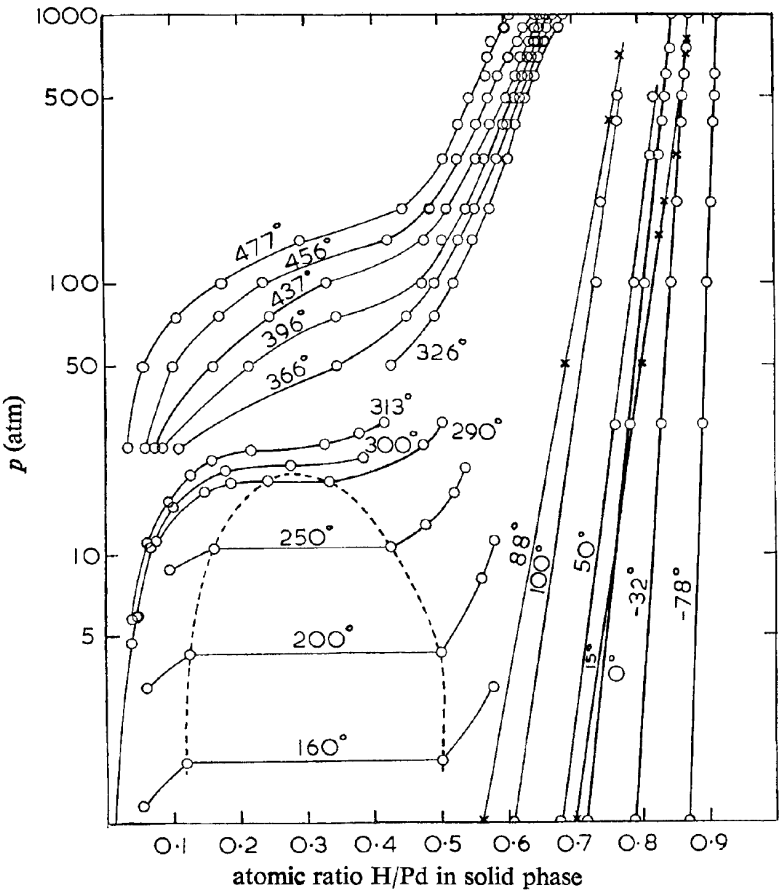

Figure 2.6: Pressure concentration isotherm [25] .

After loading, there are structural changes in the palladium. As mentioned previously, some of these changes include an increased lattice constant, embrittlement, and the volume of the palladium increases.

2.2: Pulsed power and the perturbation of the palladium hydride system

Pulsed power is the rapid release of stored energy. This, of course, results in extremely large amounts of instantaneous power. For example, the largest pulsed power system is Sandia Labs Z-machine which has a peak power of greater than 200 TW [26]. Pulsed power has wide applications and has been researched in a wide variety of fields

including, “food processing, medical treatment, water treatment, exhaust gas treatment, ozone generation, engine ignition, ion implantation, and others” [27].

Pulsed power systems have long been used for exploding wire and z-pinch experiments [28]. A z-pinch is a cylindrical wire that is used as a load for a pulsed power circuit. The “pinch” describes how there is a magnetic pressure due to the Lorentz force, and this force is directed toward the center of the wire which coincides with the z-axis. Therefore, due to this force directed in the z direction the name z-pinch is used. Whenever there is enough pulsed power applied to a z-pinch, the z-pinch will become a plasma.

One use of z-pinches is to produce x-rays. For example, a tungsten z-pinch can be used as a source of X-rays [29]. Additionally, using a deuterium z-pinch has been shown to produce neutrons [30]. Experimenters have used several different methods to introduce deuterium into z-pinches. Techniques have included gas puff, deuterium loaded fibers, and cryogenically formed solid deuterium z-pinches [31, 32]. The gas puff is a technique in which the gas is released at a very high pressure by a fast acting value so that there is very little transverse motion [30]. Development of neutron sources is important because neutron sources are not readily available, and there are very important applications, such as neutron capture therapy, that must have a neutron source [33]. Neutron capture therapy is a cancer treatment where a Boron 10 isotope is placed next to a cancer cell then a neutron is directed at the Boron 10 which captures the neutron to create Boron 11. The Boron 11 isotope will then decay into Lithium 7 and an alpha particle. By using this therapy, it is possible to destroy cancer cells without significantly damaging normal tissues [34].

Our research presented in this work combines pulsed power and a palladium hydride system. Even though palladium and its uses have been studied for many years, there are many phenomena left to be researched. For example, we have found very little in the literature describing the use of deuterium loaded palladium for z-pinches, likely due to palladium's high Z number and concerns of excessive radiative losses during z-pinch. In this study, we subject deuterium loaded palladium wires to a fast rise time, high power pulse, without sufficient energy to melt the wire. Such a pulse may be suitable for use as a pre-pulse in a z- pinch experiment, in which deuterium is liberated from the palladium prior to the main power pulse, and therefore could be used to produce neutrons. However, it was discovered that when a deuterium loaded palladium wire was pulsed nanoporous palladium was created. It is this result, the creation of nanoporous palladium, that is discussed in detail throughout this work.

Chapter 3: Experimental Methods

3.1: Pulsed power system

The experiments presented in this work used a low energy pulsed power system. The pulsed power system was designed to deliver an amount of energy that would be just enough to melt a palladium wire assuming that no heat was being transferred to the surroundings from the wire. Admittedly, this is an ideal situation and represents the minimum possible energy required to melt the wire. However, in any real experiment there will be some heat transfer, mainly due to convection, and taking this heat transfer into account from the wire to the surroundings would result in no melting of the wire. The intent was to deliver as much energy as possible without actually melting the wire. Thus, the minimum energy required to melt the wire was calculated as follows:

First the volume was calculated for the cylindrical wire,

$$V = h\pi r^2 = (4\ cm)\times(\pi)\times(25\ \mu m)^2 \approx 7.36\times10^{-5}\ cm^3 \tag{3.1}$$

Given that the density of palladium is $12.023\frac{g}{cm^3}$, this would yield a total mass of the wire as,

$$m = 12.023\ \left(\frac{g}{cm^3}\right)\times 7.36\ (cm^3) = 0.944\ mg \tag{3.2}$$

The melting point of palladium is 1555 °C and room temperature is 25 °C.

Subtracting the two temperatures gives the temperature change that is required to go from room temperature to the melting point which is 1530 °C. Using the fact that the specific

heat of palladium is $0.244 \ \left(\frac{J}{g°C}\right)$ at 25 °C, then the heat required to raise the temperature of the palladium to the melting point can be found as follows,

$$Q_{room} = cm\Delta T = 0.244 \ \left(\frac{J}{g°C}\right) \times (0.944\, mg) \times (1530\ °C) = 0.353\, J, \textit{ where } Q_{room} \textit{ is the heat, c is the specific heat, m is the mass, and } \Delta T \textit{ is the change in temperature.} \quad (3.3)$$

Using the fact that the atomic mass of palladium equals $106.42 \ \left(\frac{g}{mol}\right)$, we can calculate the moles of palladium as follows,

$$moles\ of\ palladium = \frac{0.994\, mg}{106.42 \ \left(\frac{g}{mol}\right)} = 8.87 \times 10^{-6}\, mol \quad (3.4)$$

Next, the energy required to break the chemical bonds at the melting point and allow for the solid palladium to undergo a phase change and become liquid palladium will be calculated. Using the heat of fusion for palladium, the heat required to cause the phase transition can be found by the following,

$$Q_{phase} = Q_{fusion} \times Pd_{mol} = 16700 \left(\frac{J}{mol}\right) \times 8.87 \times 10^{-6}\, mol = 0.148\, J \quad (3.5)$$

Adding the two energies together gives the total amount of energy to melt the palladium wire at room temperature.

$$Q_{total} = Q_{room} + Q_{phase} = 0.353\, J + 0.148\, J = 0.501\, J \quad (3.6)$$

Therefore, the pulsed power circuit was designed to deliver 0.5 J of energy to a palladium wire, and so the simple capacitive pulsed power circuit as show in *Figure 3.1* was chosen for the design of the pulsed power system. In this type of circuit, the

capacitor and supply voltage must be chosen correctly to deliver the correct energy to the wire. The formula that is used to calculate the energy stored in a capacitor is:

$$E = \frac{1}{2}CV^2 \tag{3.7}$$

where E is the energy, C is the capacitance, and V is the voltage across the capacitor.

A value of 20 kV was chosen as a supply voltage. This supply voltage is necessary to create the enormous instantaneous power of the circuit, and also allows for the use of a spark gap as a switch in the circuit (i.e. in order for current to flow across the gap between to electrodes the voltage must be relatively high). Using this fact, and then solving *equation (3.7)* for the capacitance yields,

$$C = \frac{2E}{V^2} = \frac{2(0.5\,J)}{(20\,kV)^2} = 2.5\,nF \tag{3.8}$$

Therefore, a 2.5 nF capacitor at a rated voltage of 40 kV was chose for the circuit. The 40 kV voltage rating was chosen to give a 100% margin of safety. The 5 kΩ high power resistor was chosen to protect the high voltage power supply from excessive current. The 1.6 uH of inductance in series with the wire was the circuits inductance and was largely a result from the wire holder which was several inches long due to its use in the calorimetry experiment later in this thesis, and therefore, had a large loop area.

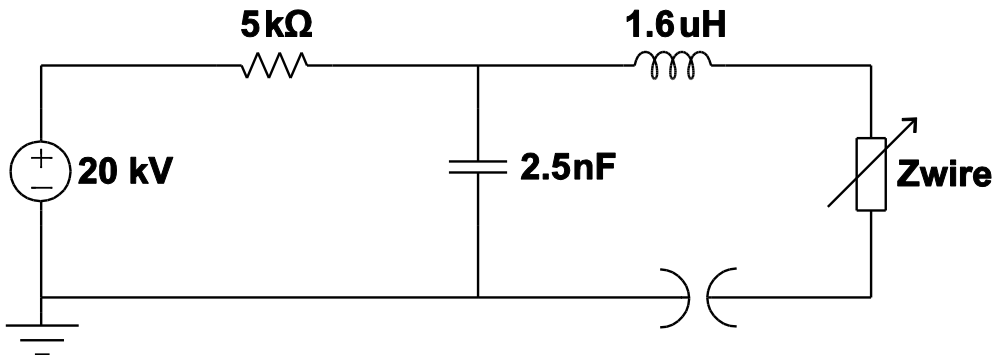

Figure 3.1: Schematic of Pulsed power circuit.

The spark gap was pressurized using nitrogen gas, and was used as a switch by releasing the pressure via an electrical switch thereby causing current to flow across the electrodes of the spark gap. The power supply was a Glassman brand high voltage power supply, and the capacitor used was a Sprague brand capacitor. Next, the circuit's function in *Figure 3.1* will be analyzed.

First, the spark gap is pressurized with 80 psi of nitrogen gas and then the power supply is set to 20 kV. This causes current to flow from the power supply, through the resistor, and into the capacitor where it charges the capacitor to 20 kV in approximately 63 μs. The power supply's output current can then be turned off, and when ready, the wire can be pulsed by releasing the pressure in the spark gap. The pressure release is controlled by an electrical switch that opens a value. This release of pressure lowers the breakdown voltage across the spark gap thereby allowing current to flow. When the pressure release value is opened, current flows from the capacitor, through the inductance of the circuit, through the palladium wire, and then through the spark gap. The discharge circuit is a resistor, inductor, and capacitor (RLC) circuit. An RLC circuit has a natural

response that is a damped oscillation. The frequency of this oscillation can be calculated by the following equation:

$$f_r = \frac{0.159}{\sqrt{LC}} = \frac{0.159}{\sqrt{(1.6\ \mu H)(2.5\ nF)}} = 2.51\ MHz \qquad (3.9)$$

An unloaded palladium wire was used and the measurements were taken using a Tektronix TDS 3052B oscilloscope, a Tektronix high voltage probe, and a Pearson's current monitoring coil. After the voltage was measured from the hot side of the palladium wire, the experiment was repeated and the voltage was measured from the ground side of the wire. The two results were subtracted from one another to yield the voltage dropped across the wire. Also, during the voltage measurements, the current through the wire was also measured.

The waveform of the voltage and also the current, *Figure 3.2* and *Figure 3.3* respectively, have a very similar shape to that of a damped oscillator with the exception that there is an added high frequency noise component that is superimposed on the lower frequency signal which can be attributed to the noise from the spark gap.

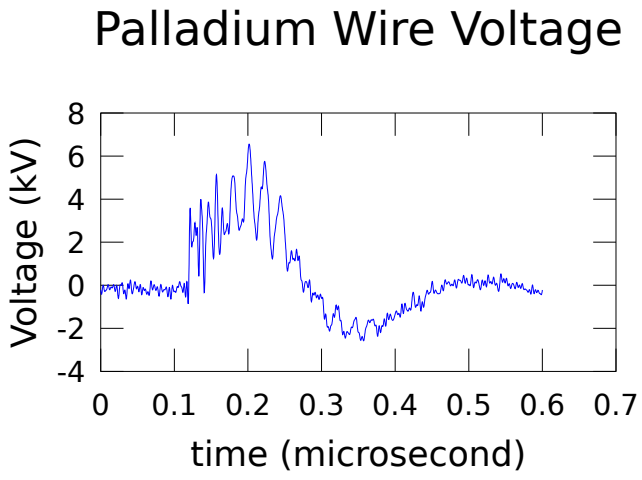

Figure 3.2: Voltage across palladium wire.

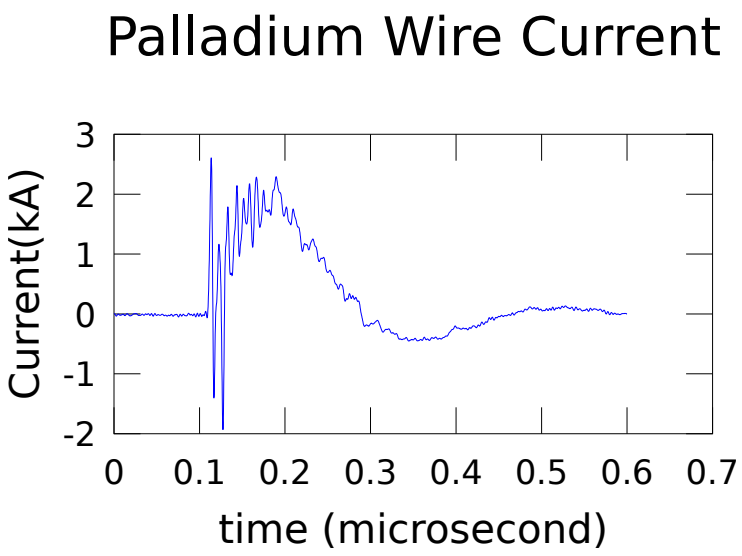

Figure 3.3: Electrical current through palladium wire.

In order to calculate the power going to the palladium wire the following equation was used:

$$P = I^2 R \tag{3.10}$$

Using this equation, the power was calculated by using the signal in *Figure 3.3* and multiplying it by 1.7 Ω, the typical resistance of a palladium wire. After the power was calculated, the resulting signal was integrated with respect to time to yield the energy delivered to the palladium wire. The energy that was calculated delivered to the wire was approximately 0.51 J which is almost identical to the expected value of 0.5 J.

By taking the current signal from the oscilloscope and performing a fast Fourier transform (FFT), we can place the signal in the frequency domain to observe the spectral data. This will allow us to observe the major frequency components of the signal. The FFT is plotted in *Figure 3.4* and shows that there is a major frequency component at 2.7

MHz. This value is very close to 2.51 MHz which is the calculated resonant frequency of the circuit.

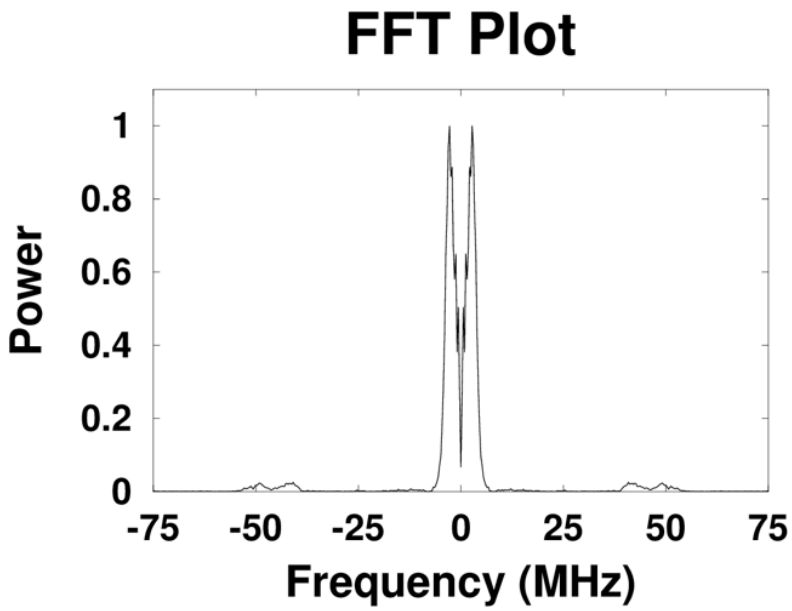

Figure 3.4: Fast Fourier Transform (FFT) of current signal.

3.2: Experimental setup

Figure 3.5 shows the experimental setup used to pulse a palladium wire in air. The elongated wire holder was necessary to facilitate wire pulsing in a liquid nitrogen bath, central to a novel diagnostic used in the calorimetry experiments describe in this work. Our overall goal was to use the pulser to supply a power pulse with low enough energy to prevent the wire from being driven into a plasma to gain an understanding of how deuterium or hydrogen would unload from the palladium wire in a prepulse type application. The instantaneous power delivered to the wire was multi megawatt, but as previously mentioned, the energy delivered to the wire was

approximately 0.5 J. Using this experimental setup, several unloaded palladium wires were subjected to the 0.5 J pulse and all the unloaded palladium wires that were tested survived being pulsed and were not melted.

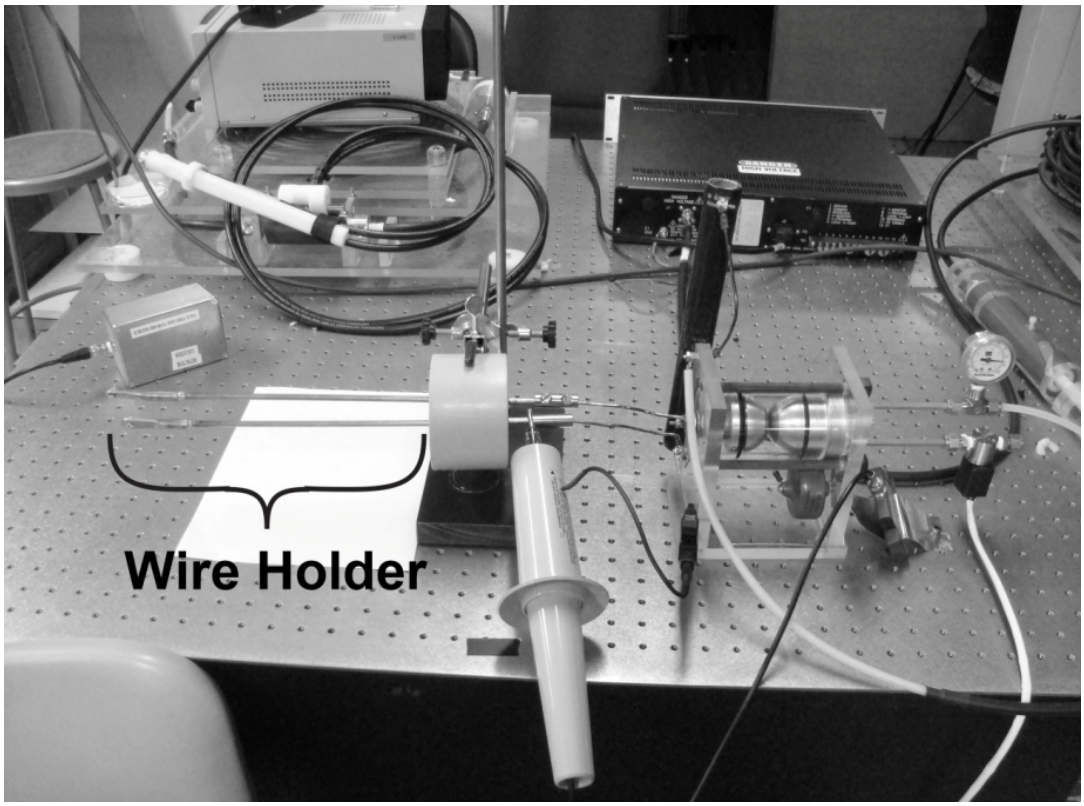

Figure 3.5: Experimental setup.

3.3: Electrochemical loading

The palladium wire that was used for the experiments was from the Goodfellow corporation and was 99.9% pure palladium of approximately 4 cm in length and 50 μm in diameter. In order for the palladium wires to undergo deuterium loading, they were placed into an electrochemical cell. Placing the palladium wire into the chemical cell

consisted of connecting one end of the palladium wire to a negative electrical potential (cathode) and the other end of the palladium wire to a coil of platinum wire that was connected to the positive potential (anode). The palladium wires were placed through the center of the platinum coil. *Figure 3.6* shows a photo of the electrochemical cell.

Figure 3.6: Electrochemical cell.

Before placing the wire into the cell, however, the wire was annealed in air which was done by passing a gradually increasing current though the wire that started from 0.5 A and went up to 0.75 A. A LabVIEW program was written to perform this annealing process in a very precise and consistent manner, and the LabVIEW code used for the annealing is shown in *appendix D*. The computer running the LabVIEW code was connected to a National Instruments BNC-2110, and one of the analog output channels of the BNC-2110 was connected to the programming current input of a KEPCO power supply which was being operated in constant current mode. In order to get the correct current out of the KEPCO, a voltage that was 1.25 times larger than the value of the desired current was applied. For example, if a current of 0.5 amps was required, then a voltage of 0.625 V was applied to the programmable input of the KEPCO. The annealing was performed to allow for some of the material defects to be removed before loading the wire with deuterium. After a wire was annealed, it was placed into the electrochemical cell, and then for deuterium loaded wires, a 20 ml of 5 x 10^{-5} M $SrSO_4$ solution in heavy water was added to the cell. Next, the initial resistance was determined using a four wire measurement with an Agilent LCR meter. This value was used to calculate the resistance ratio which is the ratio of the measured resistance to the initial resistance measured during loading. The resistance ratio corresponds directly to the loading ratio (atomic ratio-d/Pd) of the deuterium in the palladium [35]. *Figure 3.7* and *Figure 3.8* show the loading ratio vs resistance curve for hydrogen and deuterium respectively. Over time, the current of the cell was increased from approximately 1 mA to 8 mA. The chemical process is governed by electrochemical reactions, which are discussed later in this section. The D_2O or H_2O oxidation occurred at the platinum anode resulting in the

production of O_2 gas. At the surface of the palladium, cathode reduction occurred and the deuterium or hydrogen adsorbed at the surface diffused into the palladium lattice, and eventually some of the hydrogen or deuterium evolves into H_2 or D_2 gas.

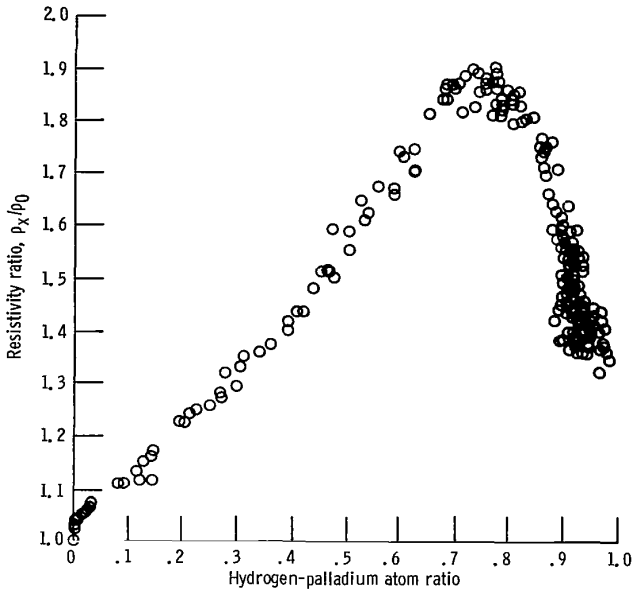

Figure 3.7: Loading curve for palladium hydride [35].

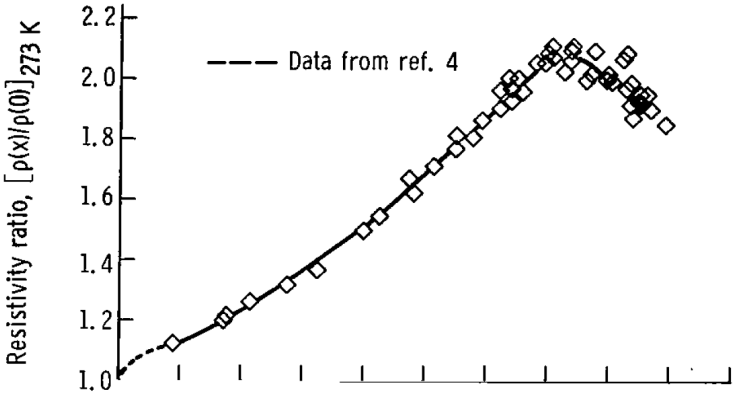

Figure 3.8: Loading curve for palladium deuteride [36].

The process by which hydrogen is discharged, adsorbed, and absorbed into the palladium is described in the following equations.

$$M + H_2O + e^- \Leftrightarrow MH_{ads} + OH^- \quad (3.11)$$

$$MH_{ads} + H_2O + e^- \Leftrightarrow M + H_2 + OH^- \quad (3.12)$$

$$MH_{ads} + MH_{ads} + e^- \Leftrightarrow 2M + H_2 \quad (3.13)$$

$$MH_{ads} \Leftrightarrow MH_{abs} \longrightarrow MH_{bulk} \quad (3.14)$$

where MH_{ads} and MH_{abs} are the adsorbed and absorbed hydrogen at the surface and just in the metal atoms respectively [37]. The reaction in *equation* (3.11) is related to electroreduction of water molecules with hydrogen adsorption at the surface of the palladium. This reaction is referred to as the Volmer reaction. The second reaction in *equation* (3.12) is related to the electrochemical hydrogen desorption which is known as the Heyrovsky reaction. The third reaction given in *equation* (3.13) is related to the chemical hydrogen desorption which is known as the Tafel reaction [38]. Finally, the last reaction in *equation* (3.14) is related to hydrogen absorption and hydrogen diffusion into the palladium [21].

In addition, 20 ml of 2.5 x 10^{-4} M Hg_2SO_4 solution in heavy water was prepared. This solution was used to seal the deuterium loaded palladium wire thereby preventing the deuterium from escaping. After the desired loading ratio was achieved, the current was gradually lowered while adding Hg_2SO_4 in 1 ml increments and gradually reducing the current until the loading ratio was stabilized. This technique follows the procedure described by McKubre, et al., [39] and is essential. Highly loaded palladium wires will deload without this step. A number of loaded palladium wires at various loading ratios

were used for the experiments as well as a number of unloaded palladium wires that were used as a control. Extremely high loading was achieved with this technique, often approaching a factor of one deuterium atom to each palladium atom. The wires were pulsed for approximately 200 ns at a voltage of 20 kV with approximately 0.5 J delivered to the wires. A similar technique was used for hydrogen loaded wires with the exception that water was used instead of heavy water for both the 20 ml of 5 x 10^{-5} M $SrSO_4$ solution and the 20 ml of 2.5 x 10^{-4} M Hg_2SO_4 solution.

3.4: Calorimetry

An unloaded 50 micrometer diameter palladium wire was connected to the pulse power system via long copper rods (i.e. the wire holder) which allowed for the wire to be placed in a Dewar filled with liquid nitrogen. This was done so that a when the wire was pulsed the energy would cause the liquid nitrogen to heat up and become gaseous nitrogen. After the wire was connected to the ends of the copper rods, the wire was left in the liquid nitrogen for approximately 15 minutes in order for the flow meter to begin stabilizing to the flow of the natural boil off rate of the liquid nitrogen in the Dewar. The cap at the end of the copper wires had an outlet to allow the nitrogen gas to flow. After the gas exits the cap, the gas would travel through a tube long enough to ensure that the nitrogen gas would reach room temperature, and would travel into a mass flow meter that was calibrated for gaseous nitrogen at room temperature. The mass flow meter reads the flow rate in standard liters per minute (SLPM), and the data are then read and stored into a computer. This reading can then be used to determine the energy released during the

experiment. The collection of the data was accomplished by using a LabVIEW data acquisition module and a computer program written in LabVIEW.

The unloaded wires were used as a control or baseline to compare with the response from the other treatments which consisted of deuterium loaded palladium wires, hydrogen loaded palladium wires, and mercury sealed only wires. The mercury sealed only wires were made by immediately adding the mercury sulfate to the strontium sulfate solution in water. This causes only minimum loading of hydrogen into the wires (roughly less than 5% hydrogen loading). In addition, the hydrogen and deuterium loaded wires consisted of different loading ratios. For the hydrogen loaded wires, the loading ratios were 20%, 50%, 72%, 85%, and 90%. For the deuterium loaded wires, the loading ratios were 20%, 50%, 77%, 85%, and 87%. The values of 72% for the hydrogen and 77% for the deuterium corresponded to the peaks of the hydrogen loading curve and deuterium loading curve.

3.5: Statistical methods

Several samples were taken for each of the treatments and the experiment was randomized. The data were stored in comma separated variable files, and the statistics were performed using the R programming language and SPSS. The main tests performed were the analysis of variance (ANOVA) with Welch's correction, and the Dunnett's T3 post hoc test both of which provide robustness for treatments of different variances.

3.6: Surface area measurements

The debris from the pulsed wire experiments in air was collected using chemical paper folded into an envelope shape. This was done because the attraction of the debris was minimal and the envelope shape allowed for the wire to be virtually encompassed within the paper which allowed for the maximum amount of the debris to be collected for every experiment. After the debris was collected it was weighed, and the debris that was collected had its surface area measured using a machine that operates using the Brunauer-Emmett-Teller (BET) theory [40].

Chapter 4: Results

4.1: Pulsed power experiments in air

For the experimental results described in this section, wires were pulsed in air. The pulse characteristic was as described earlier in *section 3.1*. The unloaded palladium wires reacted to pulsing as expected. The scanning electron microscopy (SEM) image in *Figure 4.1* shows an example of an unloaded wire that was heated upon pulsing, but did not melt.

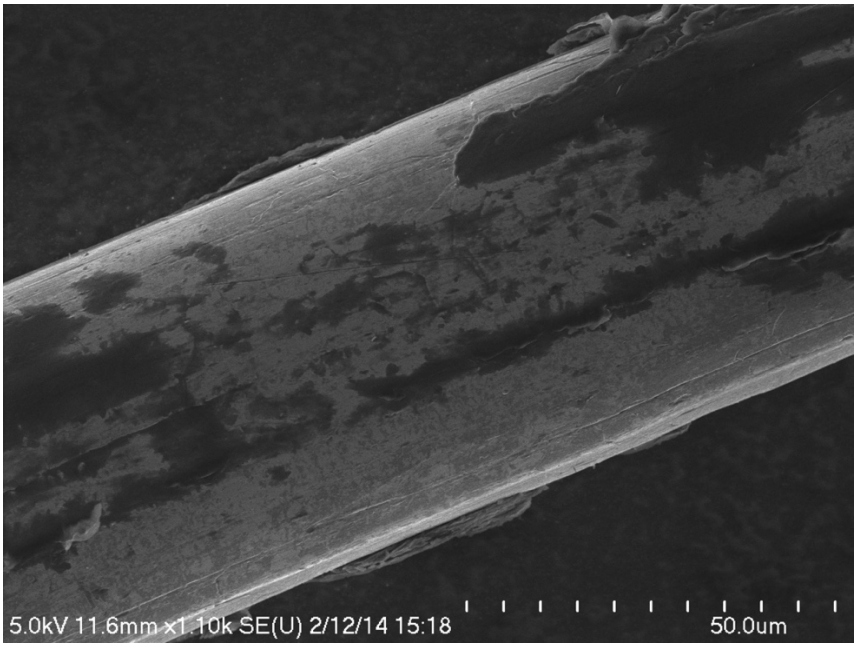

Figure 4.1: Unloaded wire after being pulsed.

The deuterium loaded wires had a dramatically different response. Upon pulsing, the deuterium loaded wires appeared to vaporize. The wire was gone and there was essentially no debris visible to the naked eye. Upon further inspection, it was discovered that the wire did not vaporize but in fact disintegrated along grain boundaries. Again,

there was not enough energy delivered to the wire to melt an unloaded wire. There was no flash characteristic of a conventionally exploded wire. This response and the results described below were and are repeatable at will and in fact have been achieved many times.

4.2: SEM images of hydrogen and deuterium loaded palladium

In order to collect the debris from the pulsed wire, a plastic specimen bag was placed over the wire prior to the wire being pulsed. The debris that was collected was then imaged using an SEM. *Figure 4.2* shows the collected debris from the pulsing of a loaded wire. Numerous particles with size dimensions on the order of 10 μm can be seen on the image.

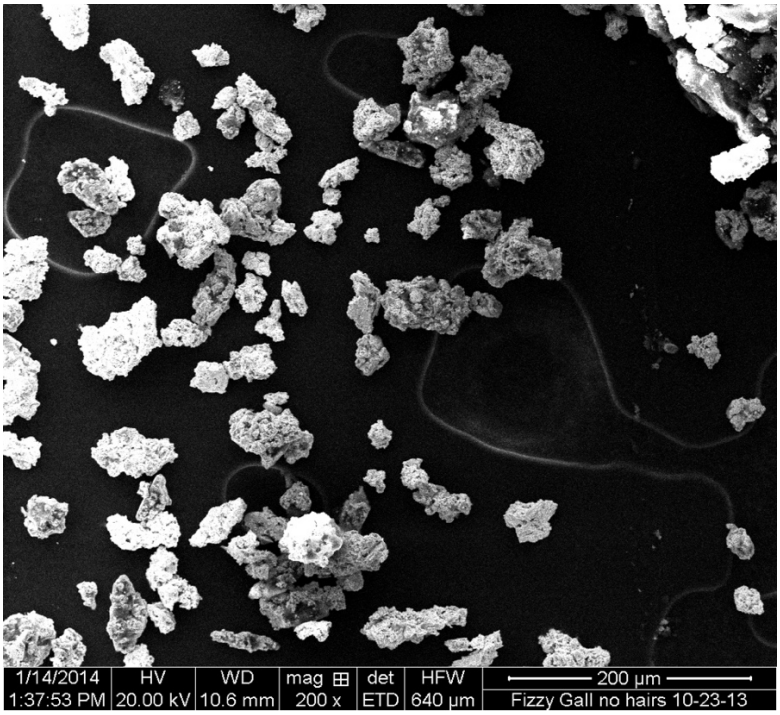

Figure 4.2: Debris left from pulsing a deuterium loaded palladium wire.

Figure 4.3 shows one particular particle under higher magnification. The SEM results show significant nanoporosity everywhere on the particle. Pitting or pores on the order of 100 nm are seen completely covering the surface of the particle. This is characteristic of all of the particles. The particles appear not to have been melted; rather it appears the particles were produced by the comprehensive and catastrophic rupture of the palladium wire.

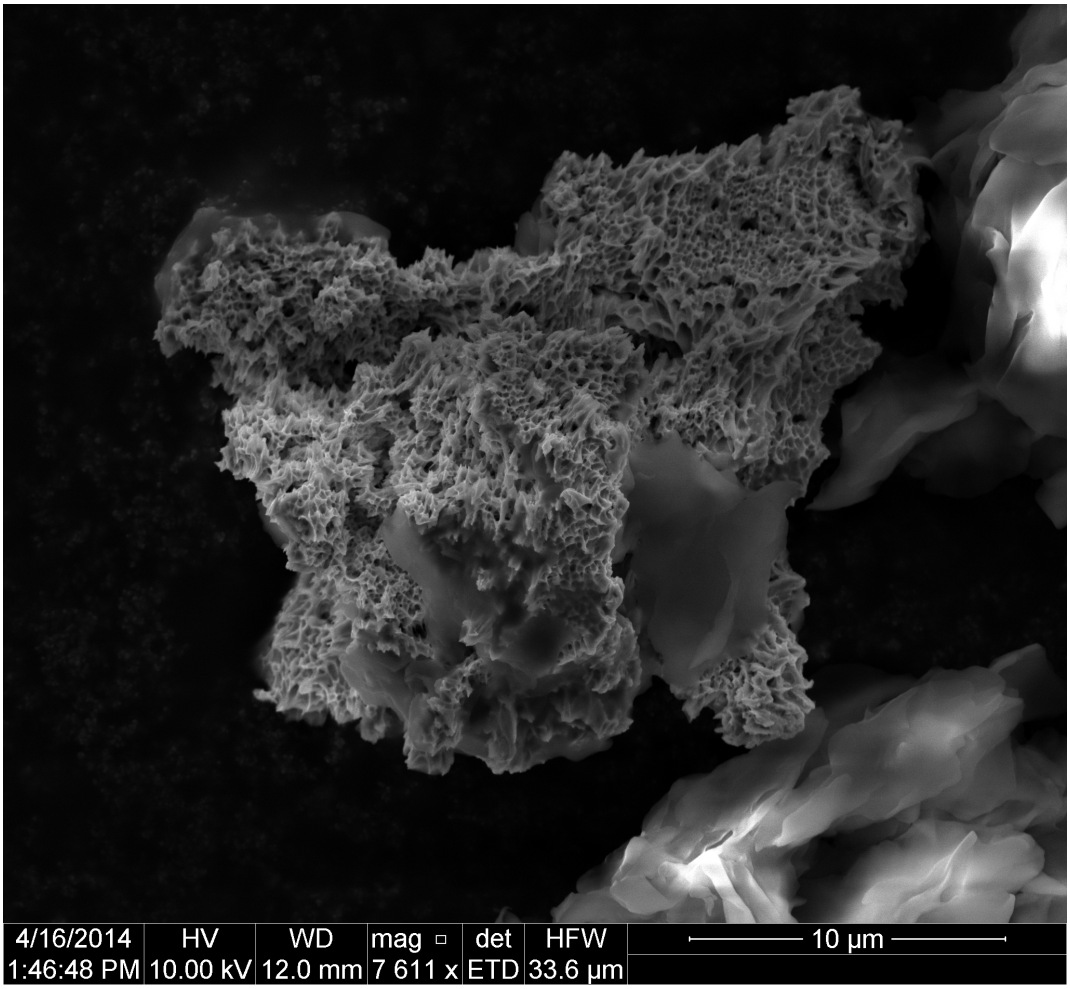

Figure 4.3: Debris from a deuterium loaded wire after wire being pulsed.

Because deuterium and hydrogen are very similar chemically, a logical experiment would be to use hydrogen loaded wires in order to see if similar results could be attained. Therefore, a palladium wire was loaded with hydrogen to a loading ratio of above 90%, and was pulsed in the same manner as was the deuterium loaded wire. The results were remarkably similar where the wire disintegrated along grain boundaries and nanoporous palladium was produced. One of the grains of nanoporous palladium was placed under an SEM and is shown in *Figure 4.4*. The amount and extent of nanoporosity is very thorough and it can be seen that there are numerous pores throughout the palladium.

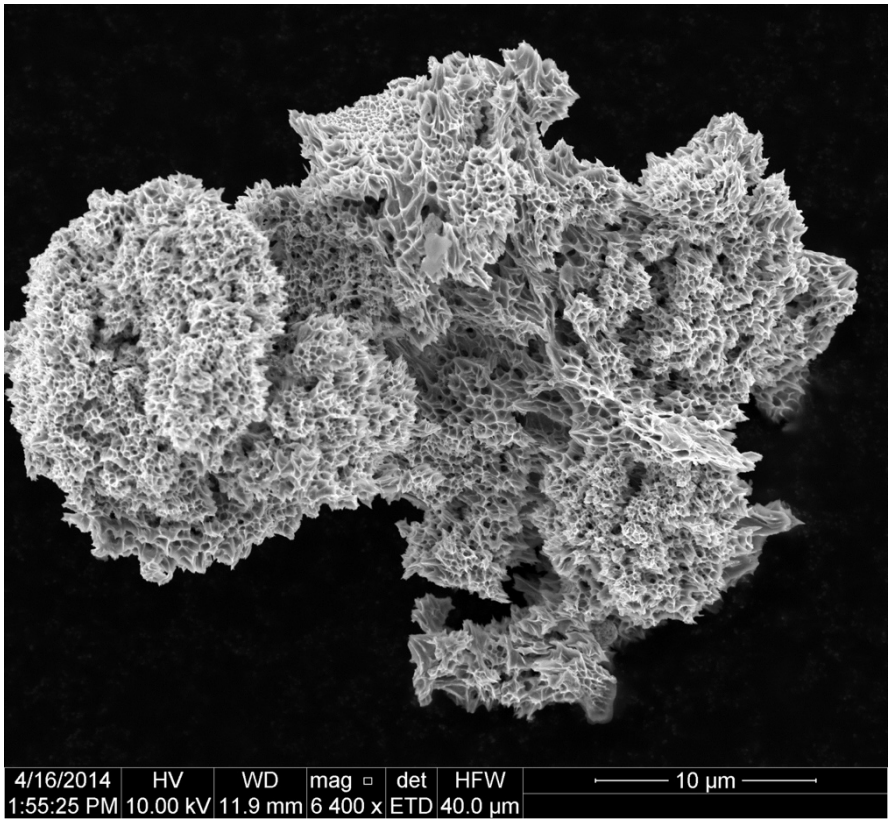

Figure 4.4:Nanoporous palladium from highly hydrogen loaded palladium wire.

The previously discussed experiments that created nanoporous palladium involved wires that were highly loaded. The next logical step is to find if there are any loading ratio thresholds where hydrogen loaded palladium began to exhibit nanoporousity.

The experiments with palladium hydride wires with varying hydrogen loading ratios were conducted with the same pulsing parameters for comparison. The experiments were conducted on single samples at each loading ratio. The debris from these experiments was analyzed using scanning electron microscopy (SEM) and energy dispersive X-ray analysis (EDAX), where only palladium was detected. In order to collect the debris from the pulsed wire, a plastic specimen bag was placed over the wire prior to the wire being pulsed. *Figure 4.5* presents SEM images of palladium hydride wires or their debris after applying an electrical pulse. The palladium hydride wires have hydrogen loading ratios of 0.5, 0.6, and 0.8, respectively.

At the hydrogen loading ratio of 0.5, there were no visible effects after pulsing; it was indistinguishable from a pulsed unloaded wire. The wire surfaces appear to be fairly smooth with no grain structures visible. However, at the loading ratio of 0.6, even though nanoporosity was not observed, we did observe the production of a large hole on the order of a few micrometers in the wire along with a noticeable change in the surface morphology. Grains of approximately ten micrometers can clearly be seen in the wire. One possibility is that the loose surface layer, resulting from oxidation in annealing and reduction in electrolysis was easily vaporized away in the wire pulsing experiment.

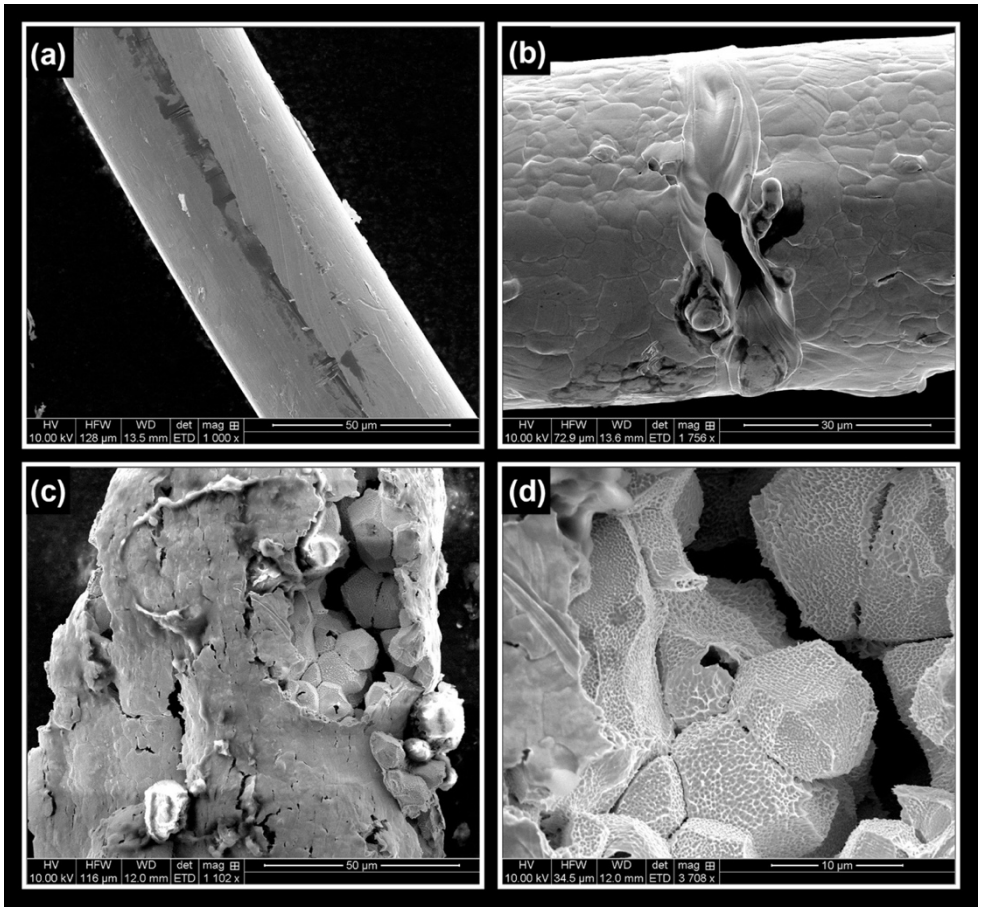

Figure 4.5: (a) 50% loaded wire after pulsing. (b) 60% loaded wire after pulsing. (c) 80% loaded wire after pulsing. (d) Higher magnication of 80% loaded wire after pulsing.

Note that the pulsed wire becomes a two-phase body, consisting of a colder core that conducts lower current, and a hot surface region which conducts most of the current [41]. The overall hydrogen loading ratio of 0.6 appears to be the threshold of breaking palladium hydride wires by electrical pulsing. Of interest is that this threshold number closely agrees with the β phase boundary of palladium hydrides. As the hydrogen loading ratio was increased to 0.8, the wire started to break apart. Most of the wire disintegrated into tiny particles with only a few small pieces of the wire remaining partially intact. As shown in *Figure 4.5 (c)*, the surface of a piece of the wire which did not completely disintegrate was broken open and parts of the inside of the wire were

ejected. The wire appears to fracture at the interface between grain boundaries, which would take less energy than a fracture of the crystal lattice structure. It was also observed that a small hole was produced at this loading ratio even within the grain, suggesting hydrogen atoms have a strong tendency to break out from the palladium hydride matrix during wire pulsing. At hydrogen loading ratios higher than 0.6, electrical pulsing of palladium hydride wires produced numerous debris (particles) with size dimensions on the order of 10 μm as observed under SEM. Further examination reveals that nanoporosity is present throughout the particles and debris. *Figure 4.6* shows SEM images of debris of exploded palladium hydride wires at loading ratios of 0.8 and 0.96, respectively. At the loading ratio of 0.8, the debris retains a granular nature but surfaces of grains became very rough with pitting-like pores of approximately 100 nm which fall into the subcategory of nanoporous material referred to as macroporous as defined by the IUPAC [42]. More micrometer sized holes were also observed within the grains. At the loading ratio of 0.96, nanoporous palladium exhibits an extensive amount of pores with pore sizes down to 100 nm. The nanopores seem to be interconnected and appear to have a complex geometry. The granular nature is no longer present and the debris appears to be continuous although the size of it is much larger (~40 μm) than the typical grain size in the original wire. This probably results from strong shocks in the electrical pulsing of the wire, which had the highest experimentally achieved hydrogen loading ratio, approaching 1. These observed experimental results indicate that the hydrogen loading ratio has significant effects on the formation of nanoporosity in palladium during electrical wire pulsing.

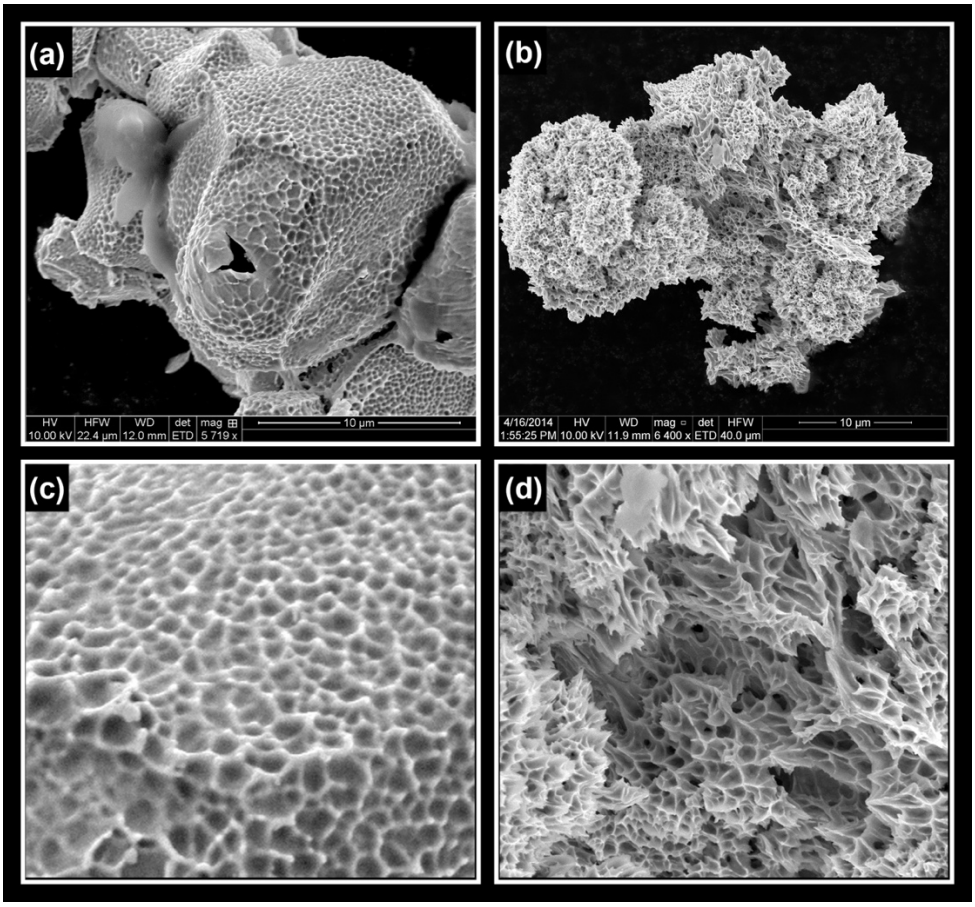

Figure 4.6: (a) SEM of debris from an 80% loaded palladium wire. (b) SEM of debris from a 96% loaded palladium wire. (c) A magnified image of Figure 3(a). (d) A magnified image of Figure 3 (b).

On one hand, the process could have been altered due to the change of the electric conductivity of the palladium hydride wires for different loading ratios. On the other hand, large amounts of hydrogen loaded in palladium could result in significant changes of the mechanical properties of the palladium hydride wires. Computer simulations show that the tensile strength of palladium hydrides decreases with increasing hydrogen loading ratios [43]. In addition, nanometric bubbles can be formed in palladium, as evidenced by experimental observations of nanobubble production during tritium storage in palladium. Tritium, a radioactive isotope of hydrogen, decays to ^{3}He, which is not soluble in palladium [44]. During an electrical pulsing, Joule heating induces a rapid

increase of wire temperature and makes palladium hydrides thermodynamically unstable. In a very short time period, hydrogen atoms would be driven out from the palladium hydrides and result in the catastrophic and comprehensive rupture of the palladium, with the resulting formation of pervasive nanoporosity in the palladium debris. It is believed that shock waves would be generated during the wire pulsing process, especially when a large amount of hydrogen is loaded. A high hydrogen loading ratio not only makes for a strong shock and explosion but the palladium hydride is also easier to break because of decreasing mechanical strength.

4.3: Calorimetry experiments

The results in *Figure 4.7* for the initial experiments utilizing unloaded and a deuterium loaded wire in the calorimeter proved interesting. When providing identical pulses of approximately 0.5 J, roughly six times more nitrogen gas flow is generated when a loaded wire is pulsed, indicating roughly 3 J of energy are released. To calculate the energy released, the flowrate was integrated from the beginning of the response curve to the peak and then the integrated value was doubled. The reason for choosing this method is because the response is not consistent after the peak of the curve (i.e. the output of the flowmeter takes different amounts of time to stabilize even among samples from the same treatment). Therefore, integrating from the beginning of the response to the peak of the curve allowed for the same limits of integration from time t_a to t_b (i.e. the same Δt). This provides for consistency throughout all the calculations, and the results using an unloaded palladium wire gave an average of 0.375 J of energy released which is 75% of the amount of energy delivered by the pulsed power system. This indicated the

diagnostic is only losing 0.125 J on average, within a 95% confidence interval (see *section 4.4*).

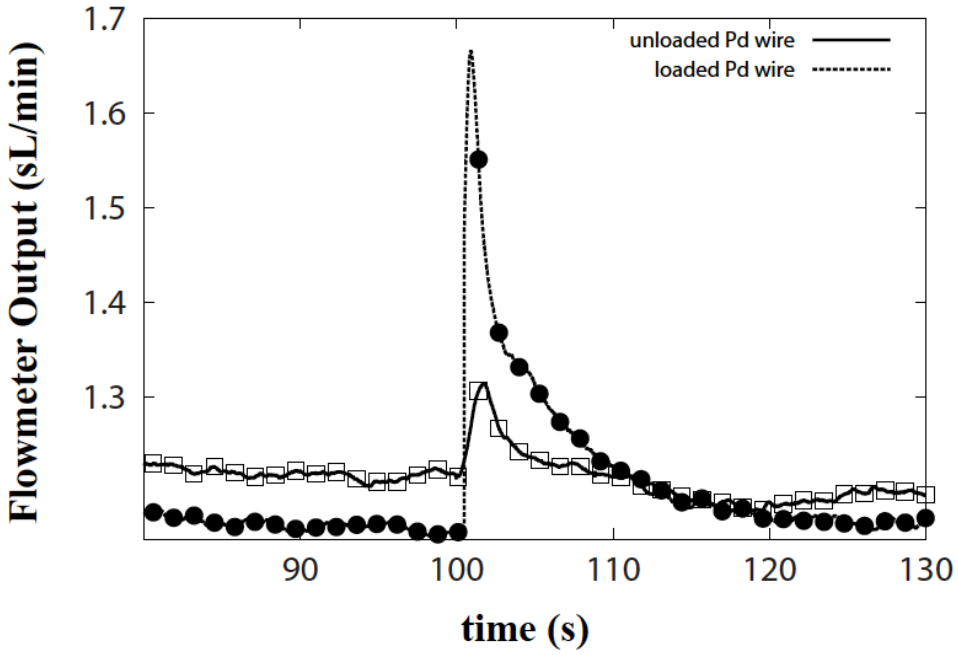

Figure 4.7: Flowmeter output of unloaded palladium wire and deuterium loaded palladium wire.

One immediate question is whether the gas flow is due to the hydrogen contained in the loaded wire. In order to calculated this, we first need to know how many moles of hydrogen there are in the fully loaded wire. This will give the maximum possible contribution to hydrogen gas in our calorimetry data. The amount of moles of hydrogen contained in a fully loaded palladium wire is the same as the moles of palladium in a wire. This number is given by *equation (3.4)* which is equal to $8.87\times10^{-6}\ mol$. Using this number and the atomic mass of hydrogen, we can then determine the mass of hydrogen by the following equation:

$$m = 1.00794\ \left(\frac{g}{mol}\right) \times 8.87 \times 10^{-6}\ mol = 8.94 \times 10^{-6}\ g \tag{4.1}$$

Using the density of hydrogen gas, we can determine the amount of hydrogen gas from the wire:

$$V = \frac{8.94 \times 10^{-6}\ g}{8.99 \times 10^{-5}\left(\frac{g}{cm^3}\right)} = 9.95 \times 10^{-2} cm^3\ or\ 0.0995\ mL \tag{4.2}$$

The amount of nitrogen gas released from an unloaded palladium wire is found by following equation using the energy released for an unloaded palladium wire equaling 0.375 J then:

$$V = 0.375\ (J) \times 4.32\left(\frac{mL}{J}\right) = 1.62\ mL \tag{4.3}$$

The energy released for a hydrogen loaded at 90 % was 1.27 J using the same equation yields:

$$V = 1.27\ (J) \times 4.32\left(\frac{mL}{J}\right) = 5.48\ mL \tag{4.4}$$

Subtracting the two gives 3.86 mL. Comparing this to the amount of hydrogen gas of 0.0995 mL means that the hydrogen gas makes up only about 2.5 percent of the total gas released during the calorimetry experiment.

Accounting for the energy released due to the exothermic deloading process at high loading ratios, as well as the energy released when atomic deuterium forms molecular deuterium, the energy released seems to be consistent with the rapid unloading of the deuterium in the wire. This result highlights the promise of this diagnostic

technique, and it was because of this it was decided that continuing with more experiments and perform a statistical analysis to look into this phenomenon might produce interesting results.

Before the statistical experiments were performed, one concern in using the diagnostic was the formation of bubbles during pulsing. If a large amount of bubbles were formed, the resulting splashing of liquid nitrogen could make difficult an accurate determination of energy delivery. *Figure 4.8* shows the glass Dewar that was employed so images of bubble formation could be made during pulsing. Additionally, *Figure 4.8* shows the steel Dewar that was used during data taking experiments. *Figure 4.9* shows an unloaded wire being pulsed, and *Figure 4.10* shows a loaded wire being pulsed. In neither case was bubble formation extensive. Bubbles rose to the surface of the liquid nitrogen near the center of the Dewar, mitigating splashing to the surface of the side walls of the Dewar.

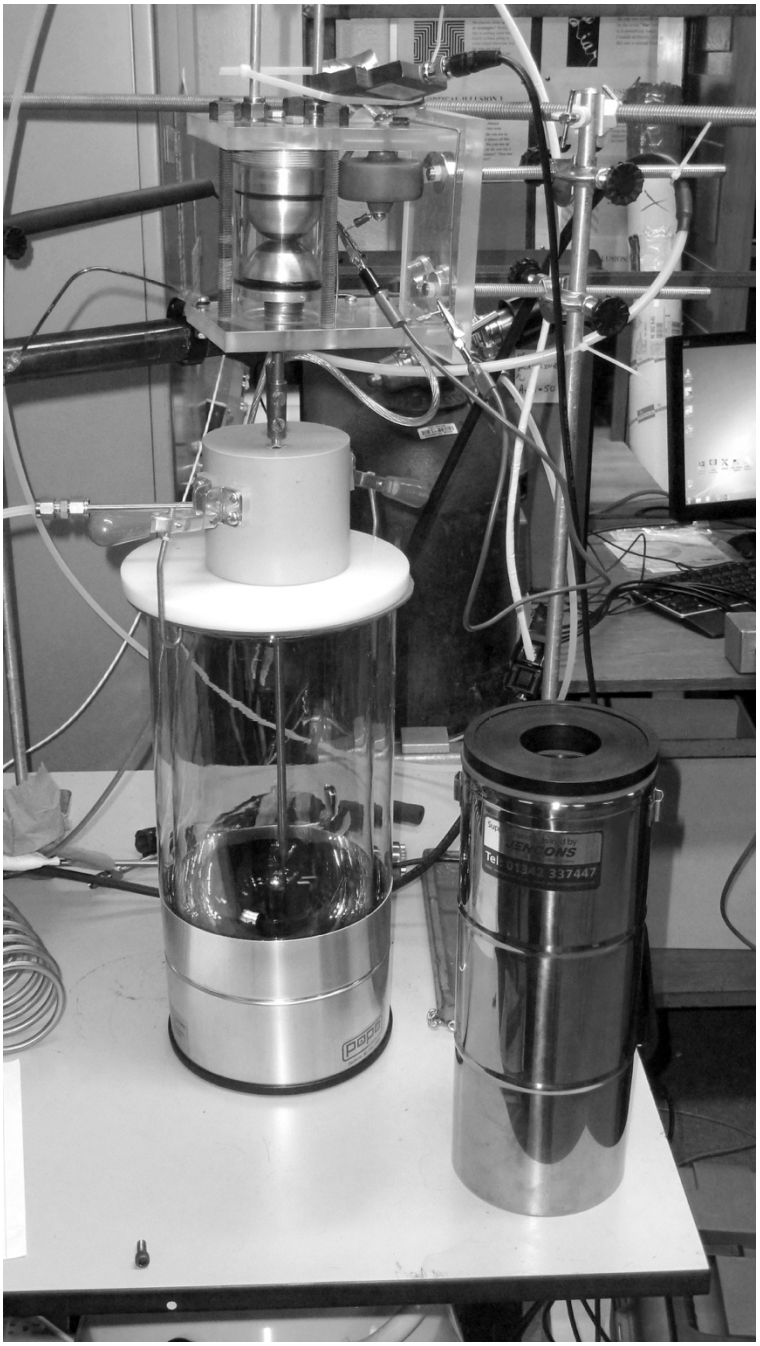

Figure 4.8: Glass Dewar on the left and the stainless steel Dewar on the right.

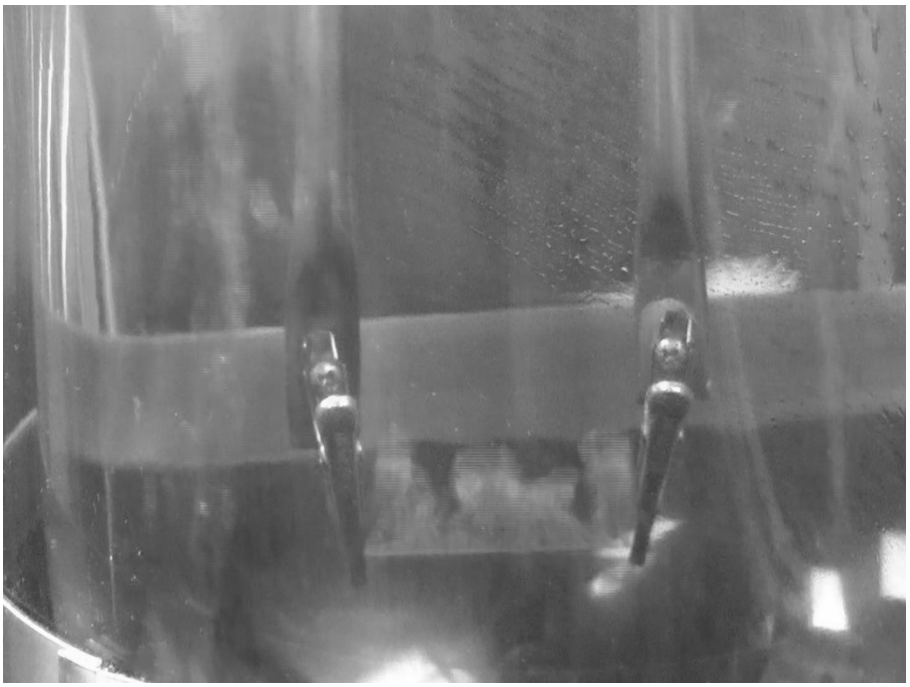

Figure 4.9: Unloaded wire after being pulsed.

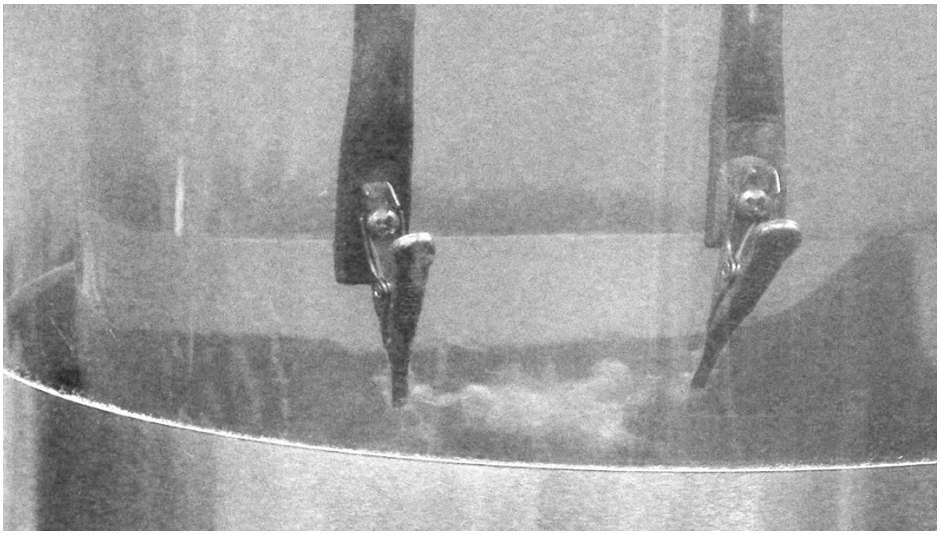

Figure 4.10: Loaded wire during pulsing.

We see in the figures that, as expected, the unloaded wire survives the pulsing with a small number of bubbles forming above the wire. In the loaded wire case, the wire seems to disintegrate. This is consistent with result of wires pulsed in air.

Next, the calorimetry was performed using several treatments. First, there was the unloaded palladium wire which was used as the control. This was compared against three other treatments: hydrogen loaded wires, deuterium loaded wires, and mercury only wires. The mercury wires were used to show if the mercury sealing, which was used in the deuterium loaded and hydrogen loaded wires, had any effects on the energy released. In addition, the experiment consisted of hydrogen and deuterium loaded wires. The hydrogen loaded wires had loading ratios of 20%, 50%, 72%, 85%, and 90%, and the deuterium loaded wires had loading ratios of 20%, 50%, 77%, 85%, and 87%. The values of 72% for the hydrogen and 77% for the deuterium corresponded to the peaks of the hydrogen loading curve and deuterium loading curve.

4.4: Calorimetry statistics

Table 4-1 shows the sample means for the hydrogen loaded wires. These point estimates of the population mean show that there is in some cases a significant difference in the energy released with an increase in hydrogen concentration in the palladium hydride wire. Likewise, *Table 4-2* shows the means for the deuterium loaded wires, and shows a similar behavior to the hydrogen wires. However, point estimates are not enough to ensure that the data are indeed statistically different. For this purpose, an interval estimate is needed.

Table 4-1

Means for hydrogen loaded wires

Sample	Energy (J)
unloaded	0.375
mercury only	1.11
hydrogen 20%	2.51
hydrogen 50%	2.21
hydrogen 72%	4.30
hydrogen 85%	3.73
hydrogen 90%	1.27

Table 4-2

Means for deuterium loaded wires

Sample	Energy (J)
unloaded	0.375
mercury only	1.11
deuterium 20%	1.97
deuterium 50%	2.72
deuterium 77%	3.59
deuterium 85%	5.54
deuterium 87%	1.87

The first analysis that was performed to determine if there were any statistical differences in the means was an *analysis of variance (ANOVA)* test with a Welch's correction. The Welch's correction was necessary due to there being different variances among the samples. For the ANOVA test, an α value of 0.05 was chosen and therefore, if a p-value is less than this value, then there exists a statistical difference between the means. The results of the ANOVA test are given in *Table 4-3*, and this table shows that the differences between some of the means were significant for both the hydrogen loaded wires and deuterium loaded wires.

Table 4-3

ANOVA with Welch's correction

Sample	p-value
hydrogen wires	< 0.05
deuterium wires	< 0.05

Now that it is has been shown that the differences between some of the means were significant, further statistical tests must be performed to compare each treatment against the control. For this statistical evaluation, the Dunnett's T3 post hoc test was used due to its robustness for treatments with different standard deviations. In the Dunnett's T3 post hoc test, a p-value of 0.05 or less shows a significant difference indicating a significant difference in the means.

Examining the hydrogen loaded wires results in *Table 4-4* shows that there exists a statistical difference between the means of the unloaded palladium wires when compared to both the palladium wires loaded with 72% hydrogen and 90% hydrogen. Also, examining the deuterium loaded wires results in *Table 4-5* shows that there exists a

statistical difference between the means of the unloaded palladium wires when compared to both the 50% deuterium loaded and the 87% deuterium loaded palladium wires.

Table 4-4

Dunnett's T3 test results for hydrogen loaded wires

Comparison	p-value
unloaded: mercury only	0.081
unloaded: hydrogen 20%	0.327
unloaded: hydrogen 50%	0.224
unloaded: hydrogen 72%	< 0.05
unloaded: hydrogen 85%	0.07
unloaded: hydrogen 90%	< 0.05

Table 4-5

Dunnett's T3 test results for deuterium loaded wires

Comparison	p-value
unloaded: mercury only	0.081
unloaded: deuterium 20%	0.543
unloaded: deuterium 50%	< 0.05
unloaded: deuterium 77%	0.063
unloaded: deuterium 85%	0.137
unloaded: deuterium 87%	< 0.05

In reference to the hydrogen loaded wires, the energy released for all except the 90% loaded and the 72% loaded wires can be explained by the formation of diatomic

hydrogen after the wire has been pulsed. That is to say, the energy due to the formation of diatomic hydrogen added to the energy delivered to the wire of 0.5 J falls within the 95% confidence interval of all the treatments except the 90% loaded and 72% loaded wires. In other words, as the hydrogen concentration is increased, more diatomic hydrogen is formed thereby increasing the energy released. The level of energy at 72% loading is approximately 1 J higher than this calculated energy within the 95% confidence interval. This could be due to other chemical reactions such as creation of ammonia which can be created due to the catalytic properties of palladium in the presence of hydrogen and nitrogen.

In regards to 90% loaded palladium hydride, the energy released seems to be significantly lower than expected. Referring to *Figure 4.6*, which shows the surface morphology for a 80% loaded and 96% loaded palladium wire subjected to the electrical pulse, it is clear that the 96% loaded sample has significantly more surface area and damage than the 80% loaded wire, and therefore, a likely cause of the lower energy detected by the calorimeter is due to a significant amount of energy going into the deformation of the metal when nanoporous palladium was created.

The data for deuterium loaded wires are very similar to what was observed with the hydrogen data. All except for the 87% loaded wire can be explained by the formation of diatomic deuterium after the wire has been pulsed. That is to say, the energy due to the formation of diatomic deuterium added to the energy delivered to the wire of 0.5 J falls within the 95% confidence interval of all the treatments except the 87% loaded wires. As the deuterium concentration is increased, more diatomic deuterium is formed thereby increasing the energy released. Again, the 87% deuterium loaded wires showed

significant damage over other loading ratios, and the cause of the lower energy detected by the calorimeter could be attributed to a significant amount of energy going into the deformation of the metal when the nanoporous palladium was created.

Another value that should be taken into account for an energy balance is the absorption enthalpy of palladium hydride. *Figure 4.11* shows the absorption enthalpy of palladium hydride as a function of concentration. In the case of the wire explosion, we are concerned with the desorption enthalpy which is the same as the absorption except that the signs are switched. Therefore, in our case, the reaction goes from an endothermic reaction for lower concentrations to exothermic for very high concentrations. However, by using data from *Figure 4.11*, it can be seen that this makes up only a small part of the energy released during the calorimetry experiment (i.e. the energy released due to hydrogen desorption is 2 percent or less compared to the amount of energy released by the formation of diatomic hydrogen).

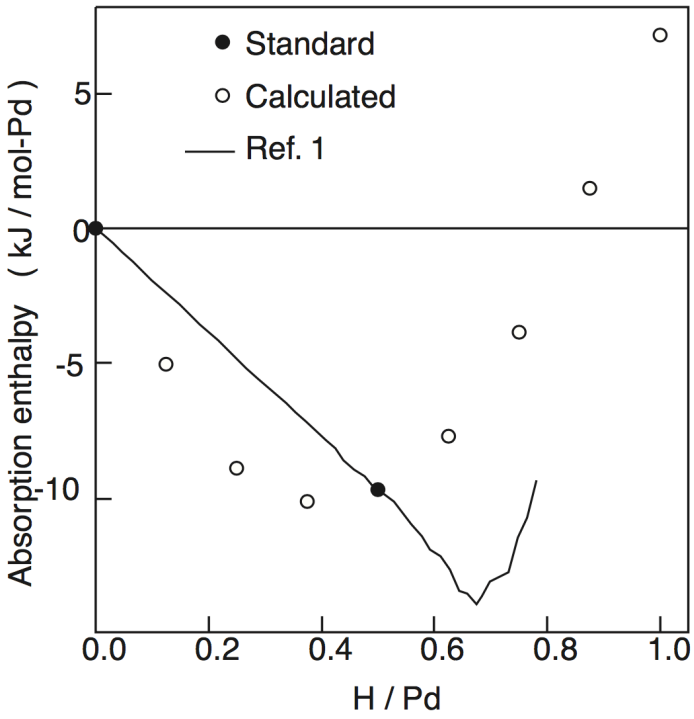

Figure 4.11: Absorption enthalpy of palladium hydride as a function of hydrogen concentration [45].

4.5: Surface area measurements

The surface area measurements where collected from the debris of highly loaded palladium hydride wires (loading ratios of approximately 90%). The palladium wires were loaded as described previously in *section 3.3* and they were pulsed in air. The debris was collected using chemical paper folded into the shape of an envelope. The chemical paper was used because it provided for a surface that allowed the palladium debris to be removed from with relative ease. After many wires debris were collected, the debris was weighted (*Figure 4.12*) and then placed into a surface area measurement machine. The surface area machine that was used was a Quantachrome Autosorb-1. The surface area is performed by first evacuating the container that contains the debris and then filling the container with nitrogen. The nitrogen adsorbs on the surface of the

debris, and the amount of gas that is absorbed is then measured which is related to the surface area of the debris. This is done via the Brunauer, Emmet and Teller or BET theory. The machine performs the measurement of nitrogen multilayer adsorption as a function of relative pressure. After the measurement is performed, an output file is created with both the graph and some important numerical results. The calculation for the surface area is performed using the standard multipoint BET procedure. There are multiple points plotted on a relative pressure plot and a linear regression line is then plotted. Both the slope of this line and the y-intercept are important quantities for calculating the surface area of the sample. The first equation used is for finding the weight of the monolayer per gram. This quantity is found instead of just the weight of the monolayer because the weight of the sample is already contained in the slope and y-intercept. This is found by using the following equations [46]:

$$\frac{W_m}{w} = \frac{1}{s+i} \quad , where\ s\ is\ the\ slope\ and\ i\ is\ the\ y-intercept \tag{4.5}$$

Plugging in the values for *s* and *I* we get:

$$\frac{W_m}{w} = \frac{1}{114.4 + 5.192} = 0.008361 \tag{4.6}$$

And then the specific surface area is found by the following equation:

$$S = \frac{W_m N A_{cs}}{M} \tag{4.7}$$

Where N is Avogadro's number, A_{cs} is the molecular cross-sectional area of the nitrogen adsorbate, and M is the molecular weight of the nitrogen adsorbate. Plugging the values in the equation yields,

$$S = \frac{(0.008361)(6.023\times10^{23})(16.2\ \text{Å}^2)}{28.0134} = 29.12\ \frac{m^2}{g} \tag{4.8}$$

The specific surface area of $29.12\ \frac{m^2}{g}$ was measured from our 19.5 mg sample of palladium nanoporous powder. This result compares favorably with results yielding a specific surface area of $23\ \frac{m^2}{g}$ and $30\ \frac{m^2}{g}$ by dealloying [47, 48]. There are clearly benefits with using our method of producing nanoporous palladium. First, the dealloying technique uses acids which require great care when using and disposing. Also, dealloying utilizes sputtering techniques which require more expensive equipment as compared to our process. Additionally, for our system, it is quite reasonable to envision a method where mercury would be unnecessary because the wire would be pulsed very quickly after loading.

If such a method is devised, the only metal left after our process would be nanoporous palladium, unlike the dealloying process which almost inevitably results in some metal contamination. With this finding, the results do look promising and there are many other experiments that can be performed with various pulsed power systems that

may lead to improved results. Moreover, other metals or alloys that have very high levels of hydrogen absorption have not been tried, and may lead to similar or better results.

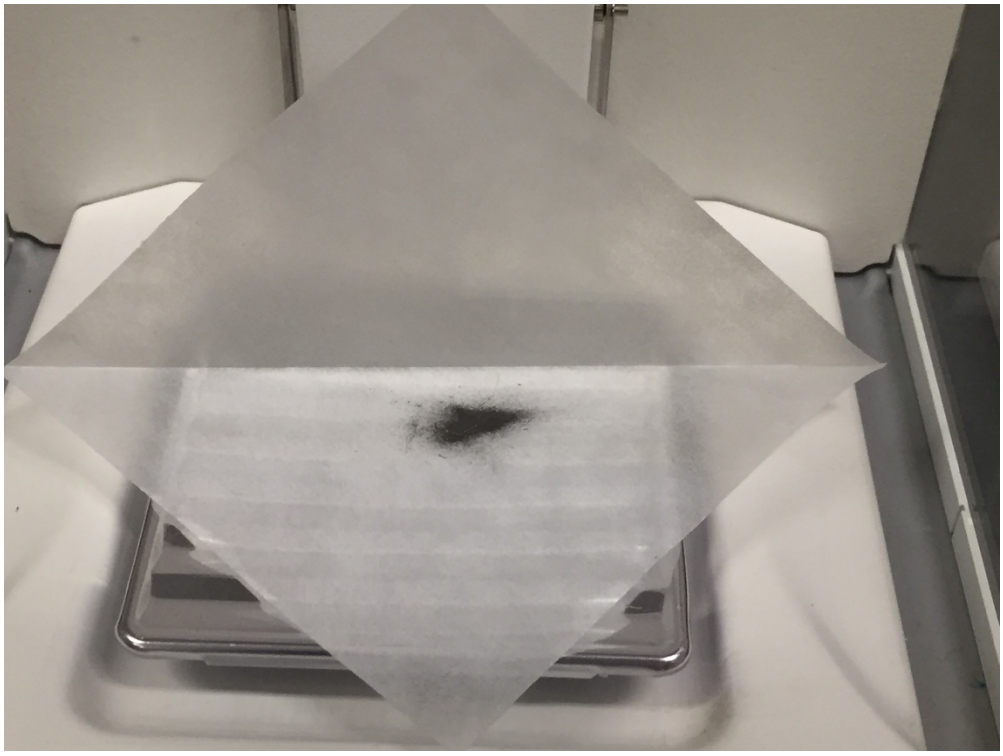

Figure 4.12: Nanoporous palladium powder being weighed.

Chapter 5: Conclusion

The technique of using pulsed power for the creation of nanoporous palladium is novel and allows for an alternative manufacturing method to dealloying, which is an involved process using techniques such as sputtering and acids. In addition, surface area measurements showed results that were comparable to and in some cases better than dealloying techniques. This is a very promising result, and shows that this method may provide a way to produce pure nanoporous palladium with less difficulty, with no metal containments, and at a lower cost.

This work describes the catastrophic and comprehensive rupture of the palladium resulting in un-melted particles exhibiting extensive nanoporosity. This result could be explained by a rapid deloading of hydrogen or deuterium out of solid solution with palladium, and seems to be consistent with the results of this experiment. Researchers have found that when storing tritium in palladium, nanometric bubbles can form in the metal [43, 44]. Tritium decays into helium-3, and helium is not soluble in palladium. The helium produced through nuclear decay comes out of the palladium lattice and forms bubbles. It is possible that when we pulse these hydrogen loaded palladium wires, we rapidly drive hydrogen out of solid solution with palladium. In this highly loaded palladium, nanometric bubbles are formed everywhere. The hydrogen in the bubbles is heated through processes like the formation of molecular hydrogen, resulting in the catastrophic and comprehensive rupture of the palladium, and the formation of the pervasive nanoporosity in the palladium debris. This process is so rapid that the palladium is not melted, and the energy is utilized to modify the surface area and create nanoporous palladium particles.

In summary, we demonstrated that nanoporous palladium with a specific surface area of 29.12 $m^2 g^{-1}$ can be created using highly loaded palladium hydride wires by applying a low energy, fast electric pulse. Hydrogen loaded in palladium significantly affects the electrical wire explosion process. At a hydrogen loading ratio below 0.6, the palladium hydride wires remain intact, whereas at hydrogen loading ratios higher than 0.6, the wires disintegrated and nanoporosity in palladium was observed. The higher the hydrogen loading ratio, the more extensive the nanoporosity produced. The novel method we used provides an alternative way to effectively produce nanoporous palladium. The results of the calorimetry experiment demonstrate the promise of this experimental technique in characterizing the energy balance of palladium wires loaded with hydrogen or deuterium that have been electrically pulsed. Images of wire pulsing in liquid nitrogen are consistent with other work reported in air, suggesting loaded wires disintegrate when pulsed. A statistical analysis using Dunnett's T3 test with a significance level of 0.05 was performed on the experimental data, and showed a statistical difference between the means of the control (i.e. unloaded palladium wires) when compared to $PdH_{0.72}$ and $PdH_{0.9}$, and a statistical difference when comparing the control mean to $PdD_{0.5}$ and $PdD_{0.87}$. The values of the energy measured by the calorimeter can be explained at least in part by the energy released during the formation of molecular hydrogen and energy going into forming the surface of nanoporous palladium.

Appendix A: BET results

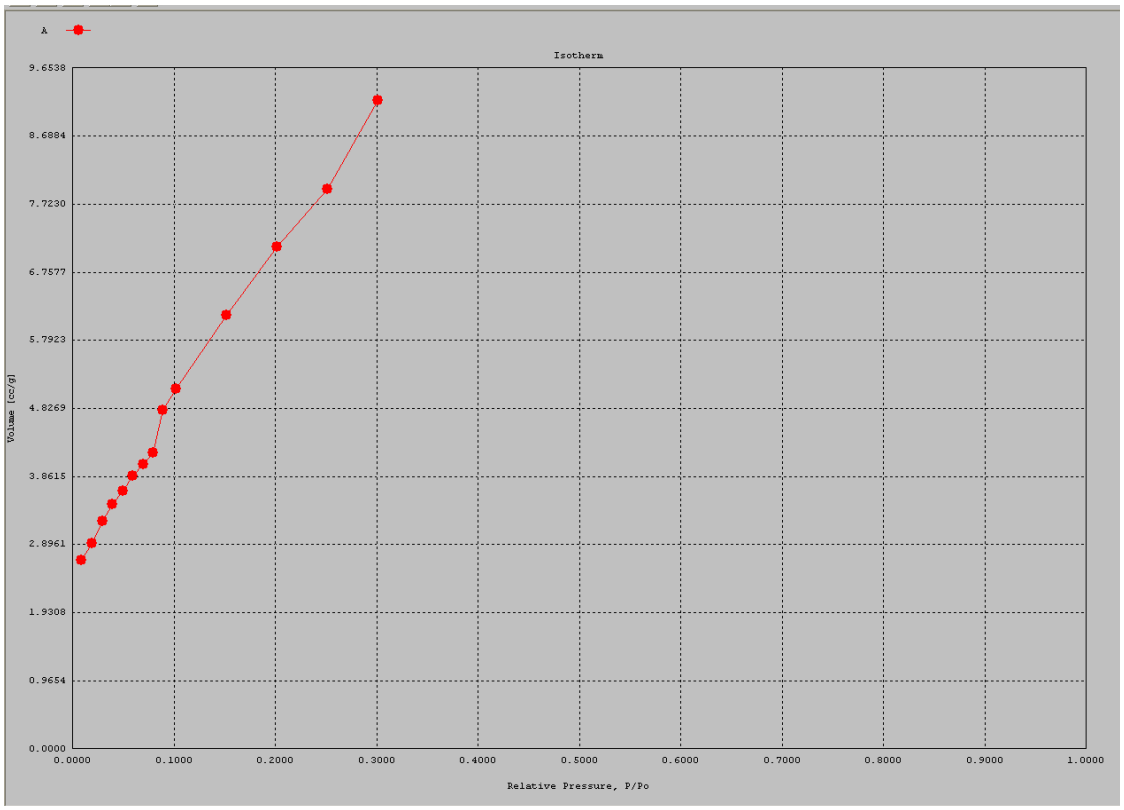

09/27/2016

Quantachrome Instruments
Quantachrome Autosorb Automated Gas Sorption System Report
Autosorb 1 for Windows 1.53

File name:	C:\QCdata\PhysData\PALLADIUM_SKNR.raw				
Sample ID:	PALLADIUM	Description:	PALLADIUM		
Comments:					
Operator:	SB	Sample weight:	0.0195 g		
Analysis gas:	Nitrogen	X sect. area:	16.2 Å²/molec	Non-ideality:	6.58e-05
Adsbate (DRP):	Nitrogen	Bath Temp.:	77.30		
Outgas Temp:	24.0 °C	Outgas Time:	4.0 hrs	Analysis Time:	261.0 min
P/Po tolerance:	0	Equil. time:	3	End of run:	09/26/2016 16:49
Station #:	1	PC sw. version:	1.53	TempComp:	Off

Isotherm

P/Po	Volume [cc/g] STP	P/Po	Volume [cc/g] STP
9.2664e-03	2.6803	1.5232e-01	6.1454
1.9908e-02	2.9097	2.0228e-01	7.1121
2.9805e-02	3.2267	2.5234e-01	7.9346
3.9866e-02	3.4622	3.0187e-01	9.1941
4.9919e-02	3.6503		
5.9876e-02	3.8766		
6.9951e-02	4.0313		
7.9913e-02	4.2008		
8.9552e-02	4.8074		
1.0281e-01	5.0995		

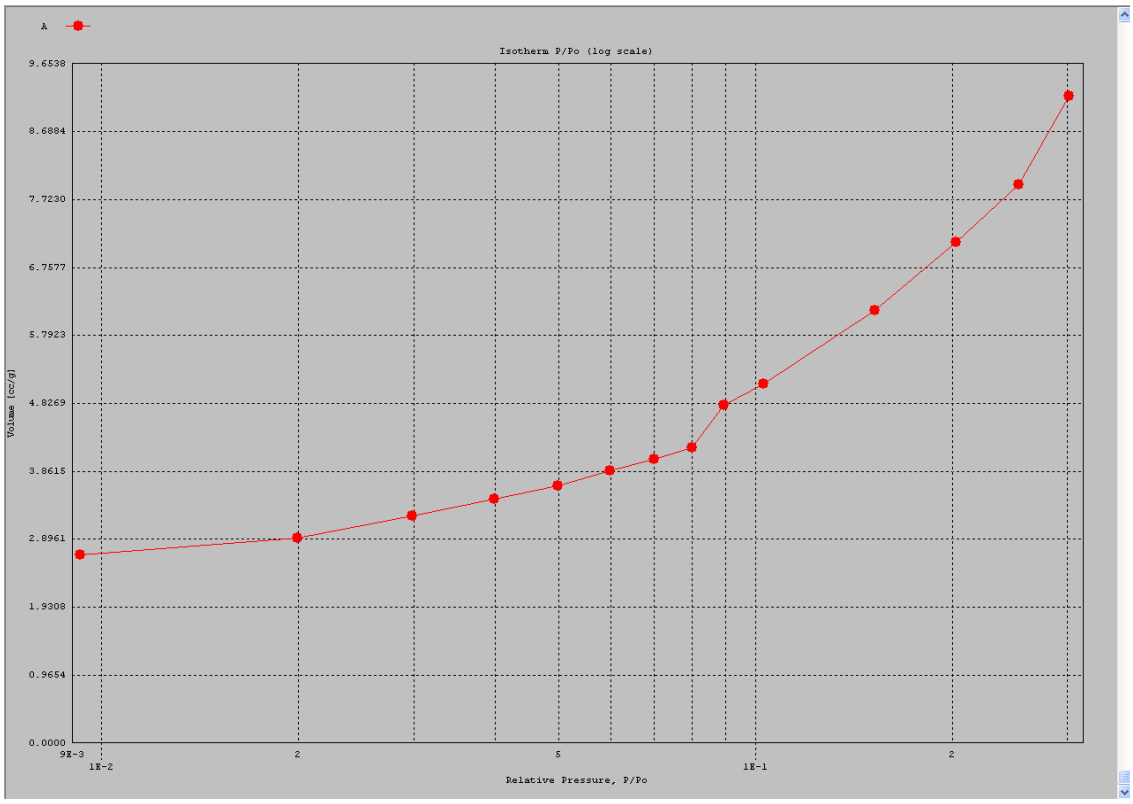
A
Isotherm P/Po (log scale)
9.6538
8.6884
7.7230
6.7577
5.7923
4.8269
3.8615
2.8961
1.9308
0.9654
0.0000
Volume [cc/g]
9E-3
1E-2
2
5
1E-1
2
Relative Pressure, P/Po

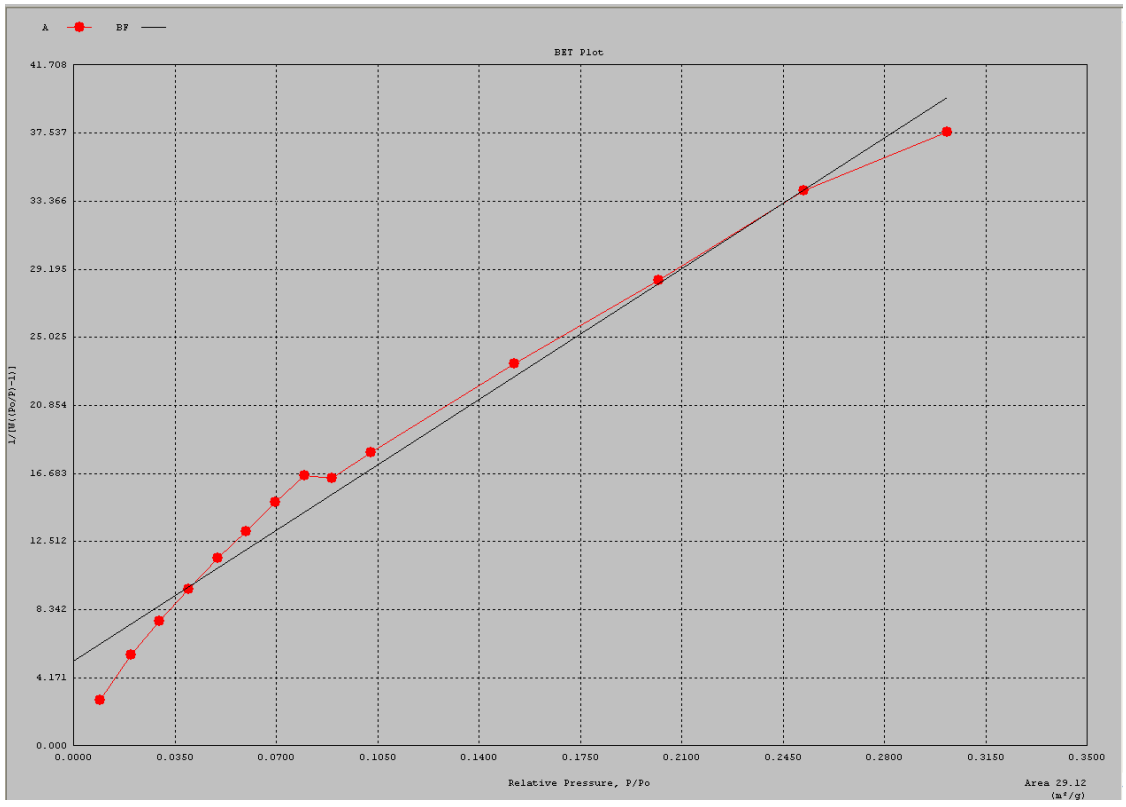
A
BF
BET Plot
41.708
37.537
33.366
29.195
25.025
20.854
16.683
12.512
8.342
4.171
0.000
1/[W((Po/P)-1)]
0.0000
0.0350
0.0700
0.1050
0.1400
0.1750
0.2100
0.2450
0.2800
0.3150
0.3500
Relative Pressure, P/Po
Area 29.12
(m²/g)

09/27/2016

Quantachrome Instruments
Quantachrome Autosorb Automated Gas Sorption System Report
Autosorb 1 for Windows 1.53

File name:	C:\QCdata\PhysData\PALLADIUM_SKNR.raw				
Sample ID:	PALLADIUM	Description:	PALLADIUM		
Comments:					
Operator:	SB	Sample weight:	0.0195 g		
Analysis gas:	Nitrogen	X sect. area:	16.2 Å²/molec	Non-ideality:	6.58e-05
Adsbate (DRP):	Nitrogen	Bath Temp.:	77.30		
Outgas Temp:	24.0 °C	Outgas Time:	4.0 hrs	Analysis Time:	261.0 min
P/Po tolerance:	0	Equil. time:	3	End of run:	09/26/2016 16:49
Station #:	1	PC sw. version:	1.53	TempComp:	Off

MULTIPOINT BET

P/Po	Volume [cc/g] STP	1/(W((Po/P)-1))
9.2664e-03	2.6803	2.792E+00
1.9908e-02	2.9097	5.585E+00
2.9805e-02	3.2267	7.618E+00
3.9866e-02	3.4622	9.596E+00
4.9919e-02	3.6503	1.152E+01
5.9876e-02	3.8766	1.315E+01
6.9951e-02	4.0313	1.493E+01
7.9913e-02	4.2008	1.654E+01
8.9552e-02	4.8074	1.637E+01
1.0281e-01	5.0995	1.798E+01
1.5232e-01	6.1454	2.339E+01
2.0228e-01	7.1121	2.853E+01
2.5234e-01	7.9346	3.403E+01
3.0187e-01	9.1941	3.763E+01

Area = 2.912E+01 m²/g

Slope = 1.144E+02

Y - Intercept = 5.192E+00

Correlation Coefficient = 0.988287

C = 2.303E+01

Appendix B: R Programming Code for Determining Energy Released

```
setwd("/Volumes/Macintosh
HD/Users/Documents/CalorimetryExperimentDissertationV1/StatisticsForWireExperime
nt/StatisticalAnalysisAndDataForPulsedWireExperiment/peakValueComparison/unloade
dWires")

source("integralFunc.R")

# load data from file

unloadedWire_5_21_15_data =
read.table("test020_unloadedWire_5_21_15.lvm",colClasses=c("NULL",NA,NA),
header=FALSE,sep="\t",skip=22)
unloadedWire_5_22_15_data =
read.table("test025_unloadedWire_5_22_15.lvm",colClasses=c("NULL",NA,NA),
header=FALSE,sep="\t",skip=22)
unloadedWire_5_23_15_data =
read.table("test027_unloadedWire_5_23_15.lvm",colClasses=c("NULL",NA,NA),
header=FALSE,sep="\t",skip=22)
unloadedWire_5_24_15_data =
read.table("test028_unloadedWire_5_24_15.lvm",colClasses=c("NULL",NA,NA),
header=FALSE,sep="\t",skip=22)
unloadedWire_5_27_15_data =
read.table("test030_unloadedWire_5_27_15.lvm",colClasses=c("NULL",NA,NA),
header=FALSE,sep="\t",skip=22)
unloadedWire_5_28_15_data =
read.table("test032_unloadedWire_5_28_15.lvm",colClasses=c("NULL",NA,NA),
header=FALSE,sep="\t",skip=22)
unloadedWire_5_29_15_data =
read.table("test034_unloadedWire_5_29_15.lvm",colClasses=c("NULL",NA,NA),
header=FALSE,sep="\t",skip=22)
unloadedWire_6_1_15_data =
read.table("test044__unloadedWire_6_1_15.lvm",colClasses=c("NULL",NA,NA),
header=FALSE,sep="\t",skip=22)
unloadedWire_6_2_15_data =
read.table("test046__unloadedWire_6_2_15.lvm",colClasses=c("NULL",NA,NA),
header=FALSE,sep="\t",skip=22)
unloadedWire_6_3_15_data =
read.table("test049__unloadedWire_6_3_15.lvm",colClasses=c("NULL",NA,NA),
header=FALSE,sep="\t",skip=22)
unloadedWire_6_4_15_data =
read.table("test052__unloadedWire_6_4_15.lvm",colClasses=c("NULL",NA,NA),
header=FALSE,sep="\t",skip=22)
```

```
unloadedWire_11_19_15_data =
read.table("test173_unloadedWire_11_19_15.lvm",colClasses=c("NULL",NA,NA),
header=FALSE,sep="\t",skip=22)

unloadedWire_11_19_15_2_data =
read.table("test175_unloadedWire_11_19_15.lvm",colClasses=c("NULL",NA,NA),
header=FALSE,sep="\t",skip=22)

unloadedWire_11_25_15_data =
read.table("test181_unloadedWire_11_25_15.lvm",colClasses=c("NULL",NA,NA),
header=FALSE,sep="\t",skip=22)

# subtract offset and select the data to analyze
lowerlimit = 0
upperlimit = 90000
offset = 1.033453
offset2 = 1.115
offset3 = 1.406
offset4 = 1.44
offset5 = 2.49
offset6 = 2.285
offset7 = 1.63
offset8 = 2.42
offset9 = 2.235
offset10 = 1.321
offset11 = 1.643
offset12 = 3.48
offset13 = 2.005
offset14 = 2.43
# unloadedWire_5_21_15

y = matrix(unloadedWire_5_21_15_data [lowerlimit:upperlimit,1])-offset
t = matrix(unloadedWire_5_21_15_data [lowerlimit:upperlimit,2])

# unloadedWire_5_22_15

y2 = matrix(unloadedWire_5_22_15_data[lowerlimit:upperlimit,1])-offset2
t2 = matrix(unloadedWire_5_22_15_data[lowerlimit:upperlimit,2])

# unloadedWire_5_23_15

y3 = matrix(unloadedWire_5_23_15_data[lowerlimit:upperlimit,1])-offset3
t3 = matrix(unloadedWire_5_23_15_data[lowerlimit:upperlimit,2])

# unloadedWire_5_24_15
```

```
y4 = matrix(unloadedWire_5_24_15_data[lowerlimit:upperlimit,1])-offset4
t4 = matrix(unloadedWire_5_24_15_data[lowerlimit:upperlimit,2])

# unloadedWire_5_27_15


y5 = matrix(unloadedWire_5_27_15_data[lowerlimit:upperlimit,1])-offset5
t5 = matrix(unloadedWire_5_27_15_data[lowerlimit:upperlimit,2])

# unloadedWire_5_28_15

y6 = matrix(unloadedWire_5_28_15_data[lowerlimit:upperlimit,1])-offset6
t6 = matrix(unloadedWire_5_28_15_data[lowerlimit:upperlimit,2])

# unloadedWire_5_29_15

y7 = matrix(unloadedWire_5_29_15_data[lowerlimit:upperlimit,1])-offset7
t7 = matrix(unloadedWire_5_29_15_data[lowerlimit:upperlimit,2])

# unloadedWire_6_1_15

y8 = matrix(unloadedWire_6_1_15_data[lowerlimit:upperlimit,1])-offset8
t8 = matrix(unloadedWire_6_1_15_data[lowerlimit:upperlimit,2])

# unloadedWire_6_2_15

y9 = matrix(unloadedWire_6_2_15_data[lowerlimit:upperlimit,1])-offset9
t9 = matrix(unloadedWire_6_2_15_data[lowerlimit:upperlimit,2])

# unloadedWire_6_3_15
y10 = matrix(unloadedWire_6_3_15_data[lowerlimit:upperlimit,1])-offset10
t10 = matrix(unloadedWire_6_3_15_data[lowerlimit:upperlimit,2])

#  unloadedWire_6_4_15
y11 = matrix(unloadedWire_6_4_15_data[lowerlimit:upperlimit,1])-offset11
t11 = matrix(unloadedWire_6_4_15_data[lowerlimit:upperlimit,2])

# unloadedWire_11_19_15

y12 = matrix(unloadedWire_11_19_15_data[lowerlimit:upperlimit,1])-offset12
t12 = matrix(unloadedWire_11_19_15_data[lowerlimit:upperlimit,2])

# unloadedWire_11_19_15_2

y13 = matrix(unloadedWire_11_19_15_2_data[lowerlimit:upperlimit,1])-offset13
t13 = matrix(unloadedWire_11_19_15_2_data[lowerlimit:upperlimit,2])
```

```
# unloadedWire_11_25_15

y14 = matrix(unloadedWire_11_25_15_data[lowerlimit:upperlimit,1])-offset14
t14 = matrix(unloadedWire_11_25_15_data[lowerlimit:upperlimit,2])


# get the max flowrate and the time in which it occurs

maxFlow = max(y)
tmax=which.max(y)

maxFlow2 = max(y2)
tmax2=which.max(y2)

maxFlow3 = max(y3)
tmax3=which.max(y3)

maxFlow4 = max(y4)
tmax4=which.max(y4)

maxFlow5 = max(y5)
tmax5=which.max(y5)

maxFlow6 = max(y6)
tmax6=which.max(y6)

maxFlow7 = max(y7)
tmax7=which.max(y7)

maxFlow8 = max(y8)
tmax8=which.max(y8)

maxFlow9 = max(y9)
tmax9=which.max(y9)

maxFlow10 = max(y10)
tmax10=which.max(y10)

maxFlow11 = max(y11)
tmax11=which.max(y11)

maxFlow12 = max(y12)
tmax12=which.max(y12)

maxFlow13 = max(y13)
```

```
tmax13=which.max(y13)

maxFlow14 = max(y14)
tmax14=which.max(y14)

t_start = tmax - 21060
t_start2 = tmax2- 21060
t_start3 = tmax3- 21060
t_start4 = tmax4- 21060
t_start5 = tmax5- 21060
t_start6 = tmax6- 21060
t_start7 = tmax7- 21060
t_start8 = tmax8- 21060
t_start9 = tmax9- 21060
t_start10 = tmax10- 21060
t_start11 = tmax11- 21060
t_start12 = tmax12- 21060
t_start13 = tmax13- 21060
t_start14 = tmax14- 21060

t_offset = t[t_start:length(t)]-t[t_start]
y_offset = y[t_start:length(y)]

t_offset2 = t2[t_start2:length(t2)]-t2[t_start2]
y_offset2 = y2[t_start2:length(y2)]

t_offset3 = t3[t_start3:length(t3)]-t3[t_start3]
y_offset3 = y3[t_start3:length(y3)]

t_offset4 = t4[t_start4:length(t4)]-t4[t_start4]
y_offset4 = y4[t_start4:length(y4)]

t_offset5 = t5[t_start5:length(t5)]-t5[t_start5]
y_offset5 = y5[t_start5:length(y5)]

t_offset6 = t6[t_start6:length(t6)]-t6[t_start6]
y_offset6 = y6[t_start6:length(y6)]

t_offset7 = t7[t_start7:length(t7)]-t7[t_start7]
y_offset7 = y7[t_start7:length(y7)]

t_offset8 = t8[t_start8:length(t8)]-t8[t_start8]
y_offset8 = y8[t_start8:length(y8)]

t_offset9 = t9[t_start9:length(t9)]-t9[t_start9]
y_offset9 = y9[t_start9:length(y9)]
```

```
t_offset10 = t10[t_start10:length(t10)]-t10[t_start10]
y_offset10 = y10[t_start10:length(y10)]

t_offset11 = t11[t_start11:length(t11)]-t11[t_start11]
y_offset11 = y11[t_start11:length(y11)]

t_offset12 = t12[t_start12:length(t12)]-t12[t_start12]
y_offset12 = y12[t_start12:length(y12)]

t_offset13 = t13[t_start13:length(t13)]-t13[t_start13]
y_offset13 = y13[t_start13:length(y13)]

t_offset14 = t14[t_start14:length(t14)]-t14[t_start14]
y_offset14 = y14[t_start14:length(y14)]

# offset maximums
tmax_offset = which.max(y_offset)
tmax_offset2 = which.max(y_offset2)
tmax_offset3 = which.max(y_offset3)
tmax_offset4 = which.max(y_offset4)
tmax_offset5 = which.max(y_offset5)
tmax_offset6 = which.max(y_offset6)
tmax_offset7 = which.max(y_offset7)
tmax_offset8 = which.max(y_offset8)
tmax_offset9 = which.max(y_offset9)
tmax_offset10 = which.max(y_offset10)
tmax_offset11 = which.max(y_offset11)
tmax_offset12 = which.max(y_offset12)
tmax_offset13 = which.max(y_offset13)
tmax_offset14 = which.max(y_offset14)



#limits of integration
a = 0
b = t_offset[tmax_offset]
b2 = t_offset2[tmax_offset2]
b3 = t_offset3[tmax_offset3]
b4 = t_offset4[tmax_offset4]
b5 = t_offset5[tmax_offset5]
b6 = t_offset6[tmax_offset6]
b7 = t_offset7[tmax_offset7]
b8 = t_offset8[tmax_offset8]
b9 = t_offset9[tmax_offset9]
```

```
b10 = t_offset10[tmax_offset10]
b11 = t_offset11[tmax_offset11]
b12 = t_offset12[tmax_offset12]
b13 = t_offset13[tmax_offset13]
b14 = t_offset14[tmax_offset14]

I <-integralFunc(t_offset,y_offset,a,b)
I2 <-integralFunc(t_offset2,y_offset2,a,b2)
I3 <-integralFunc(t_offset3,y_offset3,a,b3)
I4 <-integralFunc(t_offset4,y_offset4,a,b4)
I5 <-integralFunc(t_offset5,y_offset5,a,b5)
I6 <-integralFunc(t_offset6,y_offset6,a,b6)
I7 <-integralFunc(t_offset7,y_offset7,a,b7)
I8 <-integralFunc(t_offset8,y_offset8,a,b8)
I9 <-integralFunc(t_offset9,y_offset9,a,b9)
I10 <-integralFunc(t_offset10,y_offset10,a,b10)
I11 <-integralFunc(t_offset11,y_offset11,a,b11)
I12 <-integralFunc(t_offset12,y_offset12,a,b12)
I13 <-integralFunc(t_offset13,y_offset13,a,b13)
I14 <-integralFunc(t_offset14,y_offset14,a,b14)


scalingFactor = (1/(60*(4.32/1000)))

areaCurve= paste("Area under Curve is =", I*scalingFactor, I2*scalingFactor,
I3*scalingFactor, I4*scalingFactor, I5*scalingFactor, I6*scalingFactor, I7*scalingFactor,
I8*scalingFactor, I9*scalingFactor, I10*scalingFactor, I11*scalingFactor,
I12*scalingFactor, I13*scalingFactor, I14*scalingFactor)
print(areaCurve)

allMax = paste("All maximum values in order are:",
maxFlow,maxFlow2,maxFlow3,maxFlow4,maxFlow5,maxFlow6,maxFlow7,maxFlow8,
maxFlow9,maxFlow10,maxFlow11,maxFlow12,maxFlow13,maxFlow14)

print(allMax)
par(mai=c(2,2,2,2))


plot(t_offset,y_offset,col = "red",type="l",xlab = NA, ylab = NA,lwd=3,cex.axis=1.5)

lines(t_offset2,y_offset2,col="green",type="l",lwd=3)
lines(t_offset3,y_offset3,col="cyan",type="l",lwd=3)
lines(t_offset4,y_offset4,col="yellow",type="l",lwd=3)
lines(t_offset,y_offset,col="purple",type="l",lwd=3)
lines(t_offset6,y_offset6,col="black",type="l",lwd=3)
lines(t_offset7,y_offset7,col="brown",type="l",lwd=3)
```

```
lines(t_offset8,y_offset8,col="gold",type="l",lwd=3)
lines(t_offset9,y_offset9,col="orange",type="l",lwd=3)
lines(t_offset10,y_offset10,col="grey",type="l",lwd=3)
lines(t_offset11,y_offset11,col="wheat3",type="l",lwd=3)
lines(t_offset12,y_offset12,col="coral",type="l",lwd=3)
lines(t_offset13,y_offset13,col="pink",type="l",lwd=3)
lines(t_offset5,y_offset5,col="lightskyblue3",type="l",lwd=3)



legend(4.5,0.7,c('unloadedWire_11_25_15','unloadedWire_5_22_15','unloadedWire_5_2
3_15','unloadedWire_5_24_15',

'unloadedWire_5_21_15','unloadedWire_5_28_15','unloadedWire_5_29_15','unloadedWi
re_6_1_15',

'unloadedWire_6_2_15','unloadedWire_6_3_15','unloadedWire_6_4_15','unloadedWire_
11_19_15',
     'unloadedWire_11_19_15_2','unloadedWire_5_27_15'),
lty=c(1,1,1,1,1,1,1,1,1,1,1,1,1,1),
     lwd=c(2.5,2.5,2.5,2.5,2.5,2.5,2.5,2.5,2.5,2.5,2.5,2.5,2.5,2.5),pt.cex=1, cex=0.5,
     col=c('red','green','cyan','yellow','purple','black','brown','gold','orange','grey','wheat3',
          'coral','pink','lightskyblue3') ,bty = 'n')


title(main="Calorimetery Experiment Flowmeter Output",cex.main=3, xlab="", ylab="")
mtext("time (s)", side=1, line=4,cex= 2.5)
mtext("flowmeter output (SLPM)", side=2, line=4,cex= 2.5)


# the following is the integral function (i.e. integralFunc())

# computes definite integral

integralFunc<-function(t,y,a,b)
{

 # trapezodial rule
        temp = 0
        tsub = t[which.min(abs(t-a)):which.min(abs(t-b))]
        ysub = y[which.min(abs(t-a)):which.min(abs(t-b))]

        Fx = rep(0,length(tsub))
        for (n in 1:(length(tsub)-1)) {

        Fx[n] = ((ysub[n]+ysub[n+1])/2)
```

```
        Istep = (tsub[n+1] - tsub[n])*((ysub[n]+ysub[n+1])/2)
        Isum = Istep + temp

        temp = Isum

        }

  Isum

}
```

Appendix C: R Programming Code for statistical analysis

```
# load library
library(userfriendlyscience)

setwd("/Volumes/Macintosh HD/Users/ ")
# load data from file

data1 = read.table("peakCSVwithEnergyCorrection_V1.csv",header=T,sep=",")
attach(data1)
names(data1)
boxplot(Peak~Sample)
# Bartlett's test for homogenious variance
bartlett.test(Peak~Sample,data1)

# Ho: Mean is the same for all classes
ANOVA1 = aov(Peak~Sample)
summary(ANOVA1)

anovaLeveneData <- abs(ANOVA1$residuals)
anovaLevene <- aov(anovaLeveneData~data1$Sample)
summary1 = summary(anovaLevene)

# Anova with Welch's Correction

ANOVAwelsh = oneway.test(Peak~Sample)

# Games-Howell post hoc method
gamesHowell = posthocTGH(Peak,Sample)

# Shapiro test for normality
shapiroTest = shapiro.test(Peak[1:11])

# Q-Q plots
qqnorm(Peak[1:11])
qqline(Peak[1:11])
print(gamesHowell)
```

Appendix D: Octave Code for Electrical Characteristics of Wire Experiment

```
clc;
clear;
clf;
format long;
begin = 1;
end1 = 10000;

dataFile1 = csvread('TEK00001.csv',0,0);
dataFile2 = csvread('TEK00000.csv',0,0);
dataFile3 = csvread('TEK00003.csv',0,0);

t = dataFile1(begin:end1,1);
t2 = dataFile2(begin:end1,1);

dt = t(2)-t(1);
dt2 = t2(2)-t2(1);
fs = 1/dt;
f1 = 51*(10^9);
V1 = dataFile1(begin:end1,2);
V2 = dataFile3(begin:end1,2);
I = dataFile2(begin:end1,2.)/0.01;
V=V2-V1;

t = 0:dt:(numel(V)-1)*dt;
t_current = 0:dt2:(numel(I)-1)*dt2;

m = length(V);          % Window length
n = pow2(nextpow2(m));  % Transform length
y = fft(V,n);           % DFT
f = (0:n-1)*(fs/n);     % Frequency range
power = y.*conj(y)/n;   % Power of the DFT

y0 = fftshift(y);          % Rearrange y values
f0 = (-n/2:n/2-1)*(fs/n);  % 0-centered frequency range
f1 = f0/(1E6);
power0 = y0.*conj(y0)/n;   % 0-centered power
powernorm = power0/(max(power0));
figure(1)

plot(f1,powernorm,'k','LineWidth', 2)

axis([-75 75 0 1.1])
set(gca, 'FontName', 'Arial')
```

```
set(gca, 'FontSize', 25)
set(gca,'FontWeight','bold','Xtick',[-75,-50,-25,0,25,50,75],...
       'Ytick',[0,.2,.4,.6,.8,1]);

xlabel('Frequency (MHz)','FontSize',30)
ylabel('Power','FontSize',30)
title('FFT Plot','FontSize',40)
x = [0.62 0.56];
y = [0.77 0.77];

 saveas(gcf,'test','png');

% Eliminate higher frequency components

rightside = heaviside(f0-5*10^7);
 leftside = heaviside(-f0-5*10^7);
  both = 1-transpose(leftside+rightside);
  figure(2)

  subplot(2,1,1)
  plot(f0,both)

   y0=y0.*both;
   power2 = y0.*conj(y0)/n;

  subplot(2,1,2)
  plot(f0,power2)
  y = fftshift(y0);
  Vnew = ifft(y);

  figure(3)
  hold on
  plot(t, Vnew(1:1:length(t)),'g')

  hold off

 % for current

 m = length(I);          % Window length
n = pow2(nextpow2(m));  % Transform length
y = fft(I,n);           % DFT
f = (0:n-1)*(fs/n);     % Frequency range
power = y.*conj(y)/n;   % Power of the DFT
```

```
y0 = fftshift(y);          % Rearrange y values
f0 = (-n/2:n/2-1)*(fs/n);  % 0-centered frequency range
power0 = y0.*conj(y0)/n;   % 0-centered power
powernorm = power0/(max(power0));
figure(4)
plot(f0,powernorm)
xlabel('Frequency (Hz)')
ylabel('Power')
title('{\bf 0-Centered Periodogram}')

% Eliminate higher frequency components

rightside = heaviside(f0-5*10^7);
 leftside = heaviside(-f0-5*10^7);
  both = 1-transpose(leftside+rightside);
  figure(5)

  subplot(2,1,1)
  plot(f0,both)

   y0=y0.*both;
   power2 = y0.*conj(y0)/n;

  subplot(2,1,2)
  plot(f0,power2)
  y = fftshift(y0);
  Inew = ifft(y);

  figure(6)
  hold on
  plot(t, Inew(1:1:length(t)),'g')
  hold off

 % calculate power and energy

 R =2.663;
 Vnew = transpose(Vnew);
 Inew = transpose(Inew);
 % find upper and lower limits of time
 [rowLow,colLow]=find(t<0.6E-6);
 t_low=colLow(1,numel(colLow));
 [rowHigh,colHigh]=find(t>1.2E-6);
 t_high=colHigh(1,1);
 tnew=t(1,(t_low:t_high));
 Pcurrent = Inew(t_low:t_high).*Inew(t_low:t_high).*1.7;
 totalEnergy=trapz(t2(t_low:t_high),Pcurrent)
```

Appendix E: LabVIEW Annealing Code

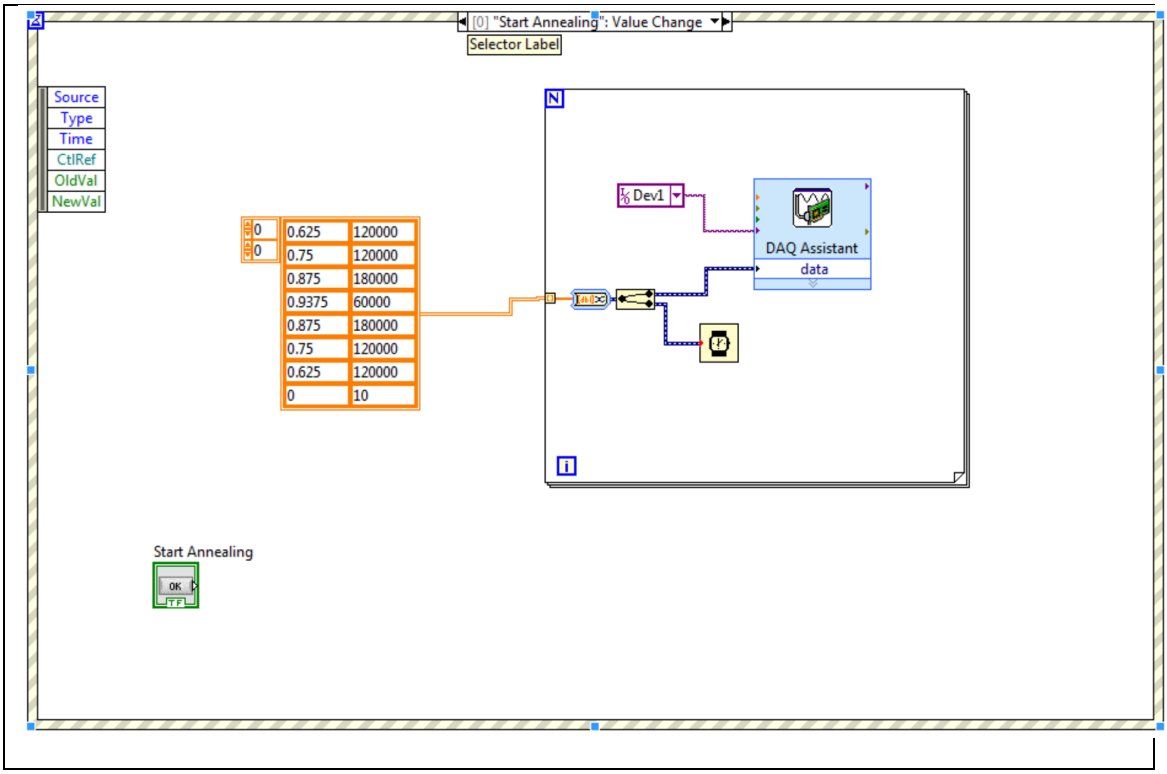

References

[1] T. Hübert, L. Boon-Brett, G. Black, and U. Banach, "Review: Hydrogen sensors – A review," *Sensors & Actuators: B. Chemical,* Review Article vol. 157, pp. 329-352, 1/1/2011 2011.

[2] M. Hakamada, H. Nakano, T. Furukawa, M. Takahashi, and M. Mabuchi, "Hydrogen storage properties of nanoporous palladium fabricated by dealloying," *Journal of Physical Chemistry C,* Article vol. 114, no. 2, pp. 868-873, 2010.

[3] D. Ding and Z. Chen, "A pyrolytic, carbon-stabilized, nanoporous pd film for wide-range H 2 sensing," *Advanced Materials,* Article vol. 19, no. 15, pp. 1996-1999, 2007.

[4] W. Li, H. Ma, L. Huang, and Y. Ding, "Well-defined nanoporous palladium for electrochemical reductive dechlorination," *Physical Chemistry Chemical Physics,* Article vol. 13, no. 13, pp. 5565-5568, 2011.

[5] M. Hakamada and M. Mabuchi, "Fabrication of nanoporous palladium by dealloying and its thermal coarsening," *Journal of Alloys and Compounds,* Article vol. 479, no. 1-2, pp. 326-329, 2009.

[6] J. Yu, Y. Ding, C. Xu, A. Inoue, T. Sakurai, and M. Chen, "Nanoporous metals by dealloying multicomponent metallic glasses," *Chemistry of Materials,* Article vol. 20, no. 14, pp. 4548-4550, 2008.

[7] D. B. Robinson *et al.*, "Scalable synthesis of nanoporous palladium powders," *International Journal of Hydrogen Energy,* Article vol. 34, no. 13, pp. 5585-5591, 2009.

[8] Y. A. Kotov, "Electric explosion of wires as a method for preparation of nanopowders," *Journal of Nanoparticle Research,* Review vol. 5, no. 5-6, pp. 539-550, 2003.

[9] G. Zheng, B. N. Popov, and R. E. White, "The Role of Thallium as a Hydrogen Entry Promoter on Cathodically Polarized HY-130 Steel," *Journal of the Electrochemical Society,* Article vol. 141, no. 6, pp. 1526-1532, 1994.

[10] C. W. F. a. T. Ludlam, "Calorimetry in High-Energy Physics," *Annual Review of Nuclear and Particle Science,* vol. 32, pp. 335-389, 1982.

[11] M. M. J. B. F. Tanzella, "HDTRA1-08-1-0050 SRI Final Report," 2011.

[12] E. M. Wise, *Palladium: recovery, properties, and uses*. New York,: Academic Press, 1968, pp. xii, 187 p.

[13] N. N. Greenwood and A. Earnshaw, *Chemistry of the elements*, 2nd ed. Oxford ; Boston: Butterworth-Heinemann, 1997, pp. xxii, 1341 p.

[14] E. Wicke, H. Brodowsky, and H. Zuechner, "HYDROGEN IN PALLADIUM AND PALLADIUM ALLOYS," *Hydrogen in Met 2,* pp. 73-155, 1978.

[15] F. A. Lewis, *The palladium hydrogen system*. London, New York,: Academic Press, 1967, pp. xii, 178 p.

[16] S. Thiébaut, B. Décamps, J. M. Pénisson, B. Limacher, and A. Percheron Guégan, "TEM study of the aging of palladium-based alloys during tritium storage," *Journal of Nuclear Materials,* Article vol. 277, no. 2-3, pp. 217-225, 2000.

[17] S. Majorowski and B. Baranowski, "Diffusion coefficients of hydrogen and deuterium in highly concentrated palladium hydride and deuteride phases," *Journal of Physics and Chemistry of Solids,* Article vol. 43, no. 12, pp. 1119-1127, 1982.
[18] F. Favier, E. C. Walter, M. P. Zach, T. Benter, and R. M. Penner, "Hydrogen sensors and switches from electrodeposited palladium mesowire arrays," *Science,* Article vol. 293, no. 5538, pp. 2227-2231, 2001.
[19] S. Mubeen, T. Zhang, B. Yoo, M. A. Deshusses, and N. V. Myung, "Palladium nanoparticles decorated single-walled carbon nanotube hydrogen sensor," *Journal of Physical Chemistry C,* Article vol. 111, no. 17, pp. 6321-6327, 2007.
[20] J. D. Holladay, J. Hu, D. L. King, and Y. Wang, "An overview of hydrogen production technologies," *Catalysis Today,* Review vol. 139, no. 4, pp. 244-260, 2009.
[21] F. R. García-García, Y. H. Ma, I. Rodríguez-Ramos, and A. Guerrero-Ruiz, "High purity hydrogen production by low temperature catalytic ammonia decomposition in a multifunctional membrane reactor," *Catalysis Communications,* Article vol. 9, no. 3, pp. 482-486, 2008.
[22] L. L. Jewell and B. H. Davis, "Review of absorption and adsorption in the hydrogen-palladium system," *Applied Catalysis A: General,* Review vol. 310, no. 1-2, pp. 1-15, 2006.
[23] F. D. Manchester, A. San-Martin, and J. M. Pitre, "The H-Pd (hydrogen-palladium) System," *Journal of Phase Equilibria,* Article vol. 15, no. 1, pp. 62-83, 1994.
[24] R. B. Schwarz and A. G. Khachaturyan, "Thermodynamics of open two-phase systems with coherent interfaces: Application to metal-hydrogen systems," *Acta Materialia,* Article vol. 54, no. 2, pp. 313-323, 2006.
[25] P. L. Levine and K. E. Weale, "The palladium + hydrogen equilibrium at high pressures and temperatures," *Transactions of the Faraday Society,* Article vol. 56, pp. 357-362, 1960.
[26] R. B. Spielman *et al.*, "Tungsten wire-array Z-pinch experiments at 200 TW and 2 MJ," *Physics of Plasmas,* Article vol. 5, no. 5 PART 1, pp. 2105-2111, 1998.
[27] H. Akiyama, T. Sakugawa, T. Namihira, K. Takaki, Y. Minamitani, and N. Shimomura, "Industrial applications of pulsed power technology," *IEEE Transactions on Dielectrics and Electrical Insulation,* Review vol. 14, no. 5, pp. 1051-1064, 2007.
[28] D. D. Ryutov, M. S. Derzon, and M. K. Matzen, "The physics of fast Z pinches," *Reviews of Modern Physics,* Article vol. 72, no. 1, pp. 167-223, 2000.
[29] M. Matzen, "Z-pinches as intense x-ray sources for high energy density physics application," ed, 1997.
[30] M. G. Haines, "A review of the dense Z-pinch," *Plasma Physics and Controlled Fusion,* Review vol. 53, no. 9, 2011, Art. no. 093001.
[31] C. A. Coverdale *et al.*, "Neutron production and implosion characteristics of a deuterium gas-puff Z pinch," *Physics of Plasmas,* Article vol. 14, no. 2, 2007, Art. no. 022706.

[32] J. D. Sethian, A. E. Robson, K. A. Gerber, and A. W. Desilva, "Enhanced stability and neutron production in a dense Z-pinch plasma formed from a frozen deuterium fiber," *Physical Review Letters,* Article vol. 59, no. 8, pp. 892-895, 1987.
[33] O. E. Kononov *et al.*, "Optimization of an accelerator-based epithermal neutron source for neutron capture therapy," *Applied Radiation and Isotopes,* Conference Paper vol. 61, no. 5, pp. 1009-1013, 2004.
[34] R. F. Barth, H. Albert, and R. G. Fairchild, "Boron Neutron Capture Therapy of Cancer," (in English), *Cancer Research,* Article vol. 50, no. 4, pp. 1061-1070, 01 / 01 / 1990.
[35] D. A. O. a. R. J. Smith, "Absorption of hydrogen by palladium and electrical resistivity up to hydrogen-palladium atom ratios of 0.97," *Nasa Technical Note D-5441,* 1969.
[36] R. J. S. D. A. Otterson, A. United States. National, A. Space, and L. R. Center, "Electrical resistivity as a function of deuterium concentration in palladium," 1968.
[37] S. Y. Qian, B. E. Conway, and G. Jerkiewicz, "Kinetic rationalization of catalyst poison effects on cathodic H sorption into metals: Relation of enhancement and inhibition to H coverage," *Journal of the Chemical Society - Faraday Transactions,* Article vol. 94, no. 19, pp. 2945-2954, 1998.
[38] F. Safizadeh, E. Ghali, and G. Houlachi, "Electrocatalysis developments for hydrogen evolution reaction in alkaline solutions - A Review," *International Journal of Hydrogen Energy,* Article vol. 40, no. 1, pp. 256-274, 2015.
[39] M. M. F. Tanzella, "HDTRA1-08-1-0050 SRI Final Report," 2011.
[40] S. Brunauer, P. H. Emmett, and E. Teller, "Adsorption of gases in multimolecular layers," *Journal of the American Chemical Society,* Article vol. 60, no. 2, pp. 309-319, 1938.
[41] B. FD, "High-temperature exploding wires," *Progress in High Temp. Phys and Chem,* vol. 2, pp. 1-63, 1968.
[42] IUPAC, "Compendium of Chemical Terminology (2nd edition). In: McNaught AD, Wilkinson A, The Gold Book. Blackwell Scientific Publications, Oxford," 1997.
[43] X. W. Zhou, J. A. Zimmerman, B. M. Wong, and J. J. Hoyt, "An embedded-atom method interatomic potential for Pd-H alloys," *Journal of Materials Research,* Article vol. 23, no. 3, pp. 704-718, 2008.
[44] A. Fabre *et al.*, "On the correlation between mechanical and TEM studies of the aging of palladium during tritium storage," *Journal of Nuclear Materials,* Article vol. 342, no. 1-3, pp. 101-107, 2005.
[45] D. Fukushi, S. Hiragi, and T. Honda, "Molecular dynamics simulation of hydrogen absorbing palladium turnover of hydrogen absorption heat into palladium," *Japanese Journal of Applied Physics, Part 1: Regular Papers and Short Notes and Review Papers,* Article vol. 39, no. 4 A, pp. 1953-1956, 2000.
[46] "Operating Manual: Quantachrome Instruments AUTOSORB-1," *P/N 05061 Rev I,* 2007.

[47] X. Wang, W. Wang, Z. Qi, C. Zhao, H. Ji, and Z. Zhang, "High catalytic activity of ultrafine nanoporous palladium for electro-oxidation of methanol, ethanol, and formic acid," *Electrochemistry Communications,* Article vol. 11, no. 10, pp. 1896-1899, 2009.

[48] E. M. Steyskal, C. Wiednig, N. Enzinger, and R. Würschum, "In situ characterization of hydrogen absorption in nanoporous palladium produced by dealloying," *Beilstein Journal of Nanotechnology,* Letter vol. 7, no. 1, pp. 1197-1201, 2016.

Vita

Julian Baker is the son of Coy Baker who resides in Louisiana, Missouri. He graduated high school from Louisiana high school in Louisiana, Missouri, and attended ITT technical institute where he graduated with an associate's degree in electronics engineering technology.

After graduating from ITT tech, he worked for the Harris corporations broadcast division where he was a test technician testing, troubleshooting, and repairing various circuit boards and modules that were a part of VHF and UHF transmitters. After working for Harris, the author worked for Garmin as an electronics repair technician repairing and troubleshooting GPS devices. It was during this time working at Garmin that the author decided to further his education by attending Johnson County Community College (JCCC). After taking several courses at JCCC, the author decided to pursue a Bachelor's degree in electrical engineering at the University of Missouri in Columbia, Missouri, where he graduated *cum laude* with a B.S.E.E. degree.

Upon graduating with a B.S.E.E. from the University of Missouri, the author worked as a circuit design engineer for Delphi on electric power steering systems (EPS). After this he decided to further his education by enrolling in the master's degree in electrical engineering program at the university of Missouri. The author's Master's thesis was entitled, *"Optimizing Antenna Gain with a Metamaterial Filter"*. After graduating with a M.S.E.E., the author decided to complete his education at the university of Missouri in the Ph.D. program for electrical engineering.